Selection of Promiscuous Anti-Cancer Phage Proteins for Tumor Targeted Nanomedicines

by

Amanda Lea Gross

A thesis submitted to the Graduate Faculty of
Auburn University
in partial fulfillment of the
requirements for the Degree of
Master of Science

Auburn, Alabama
August 1st, 2015

Keywords: Phage Display, Targeted Nanomedicines, Pancreatic Cancer, Lung Cancer, Multi-Target Selection, Tumor Heterogeneity

Approved by

Valery Petrenko, Chair, Professor of Pathobiology
Robert D. Arnold, Associate Professor of Drug Discovery & Development
Frank F. Bartol, Professor of Anatomy, Physiology & Pharmacology
Richard Curtis Bird, Professor of Pathobiology
Bruce F. Smith, Professor of Pathobiology

Abstract

Cancer remains one of the leading causes of death and requires novel approaches in both management and treatment. Tumor targeting ligands have been identified to a variety of human cancer cell lines using phage display selection techniques and used to modify current standard of care drugs and drug delivery systems with some success. However, there are still serious limitations in their use. One limitation of using targeted chemotherapy is the heterogeneity of tumor cells, both within the same tumor and across distant lesions. This heterogeneity can complicate identification of specific targeting ligands that will be effective for treating not only the primary tumor, but distant metastatic lesions. Work described below addresses the issue of tumor cell heterogeneity by using a novel, multi-target biopanning (screening) scheme involving landscape phage display libraries to select promiscuous cancer cell binding ligands. The pan-cancer binding ligands were shown to be similar to those selected previously against a variety of cancer types in addition to the cancer cell lines screened in this study. Phage displaying the fusion peptides GSLEEVSTL and GEFDELMTM were used to modify liposomal doxorubicin and the modified liposomes showed an increase of cytotoxicity of up to 8.1-fold in several lung and pancreatic cancer cell lines. Results indicate that a multi-target cell phage screening can be used effectively in heterogeneous tumor cell populations for identification of promiscuous cancer cell binding ligands.

Acknowledgements

First, I would like to thank my mentor, Dr. Valery Petrenko, for accepting me into his laboratory and passing his knowledge onto me. I would also like to thank my committee members, Drs. Robert Arnold, Frank Bartol, Curtis Bird and Bruce Smith, for all their guidance and enthusiasm to push my knowledge forward. Additionally, Dr. Deepa Bedi and James Gillespie, both whom made me feel like part of the laboratory family and taught me well. To everyone else in the laboratory (past and present), Dr. Anatoliy Puzyrev, Natasha Petrenko, Logan Stallings, as well as the long list that follow them, thank you for always making the sometimes long days more entertaining.

Finally, I would like to thank my friends and family. Thank you for always putting up with my random outbursts of science and the many long and stressful days in this process. I will always appreciate the advice, support, patience and hours spent listening to me complain. It was definitely all worth it in the end.

Table of Contents

List of Tables

List of Figures

List of Abbreviations

Ab/Am	Antibiotic/antimycotic
BSA	Bovine serum albumin
CHAPS	3-[3-Cholamidopropyl) dimethylammonio]-1-propanesulfonate
DMEM	Dulbecco's Modified Eagle's Medium
DSPE-PEG	1,2-distearoyl-sn-glycero-3-phosphoethanolamine-N-[amino(polyethylene glycol)-2000]
DSPC	1,2-distearoyl-sn-glycero-3-phophocholine
EDTA	Ethylenediaminetetraacetic acid
EGF	Epidermal growth factor
EMEM	Eagle's Minimal Essential Medium
FBS	Fetal bovine serum
EPR	Enhanced permeation and retention
IF	Infective form
MTT	3-(4,5-dimethylthiazol-2-yl)-2,5-diphenyltetrazolium bromide
NSCLC	Non-Small Cell Lung Cancer
PBS	Phosphate buffered saline
PCR	Polymerase chain reaction
PDA	Pancreatic Ductal Adenocarcinoma

PEG	Polyethylene glycol
PEW	Post elution wash
RF	Replicative form
RB	Retinoblastoma
SAE	Small airway epithelial cells
SDS	Sodium dodecyl sulfate
siRNA	Small interfering RNA
TBS	Tris buffered saline

Chapter 1:
Introduction and Literature Review

1.1 Cancer

Cancer is the second leading cause of death in the United States, claiming over 500,000 lives annually, with lung and pancreatic cancer accounting for approximately 27% and 7% of those deaths, respectively (1). The most common type of pancreatic cancer is invasive ductal adenocarcinoma (PDA), which is characterized by well-developed granular structures in desmoplastic stroma (2). Desmoplastic stroma, which is composed of a complex extracellular matrix, fibroblasts, inflammatory cells and endothelial cells. This condition leads to significantly increased interstitial pressure within the tumor (3). This dense extracellular matrix and increased surface pressure, caused by a decrease in sonic hedgehog signaling in the tumor (4), can cause constriction of the tumor vasculature, making pancreatic tumors more difficult to treat (5). Lung cancer is divided into two categories, Non-Small Cell Lung Cancer (NSCLC) and Small Cell Lung Cancer, based on biology, therapy and prognosis, with NSCLC making up approximately 85% of all lung cancer cases (6). In both PDA and NSCLC, patients are diagnosed with advanced stage cancer, often characterized by widespread metastases and limited treatment options.

1.1.1 Genetic Alterations in Cancer

Genetic alterations of proliferation control genes found in neoplastic cells can provide insight into the genetic basis of cancer. These alterations can be separated into four major categories: subtle sequence changes, alteration in chromosome number,

chromosome translocations and gene amplifications (7). Subtle sequence changes involve base substitutions, deletions, or insertions of a few nucleotides that alter the transcription of a gene. An example of this is missense mutations in the K-*ras* gene in the majority of pancreatic cancers (8). Alterations in chromosome number occur in nearly all human tumor types and result from gains or losses of entire chromosomes (9). Chromosome translocations are either fusions of different chromosomes or of two non-contiguous portions of a single chromosome (7). Finally, gene amplifications are copy number increases in regions of a chromosomal arm, resulting in increased expression of certain genes (10). There is considerable intra-tumoral genetic variation present; however the mechanism responsible for this genetic diversity is still unclear. Intra-tumoral genetic diversity plays an important role during tumor development which allows the resulting tumor cells to respond accordingly to different selective and therapeutic agents (11).

1.1.2 Lung Cancer

Genetic changes in NSCLC are multiple, complex and heterogeneous (12). Included are p53, $p16^{INK4A}$ and *Ras* mutations. Typically, p53 regulates expression of downstream genes that control cell-cycle checkpoint signals causing cells to either undergo G1 arrest, which allows for DNA repair, or apoptotic cell death (13). Mutations to p53 allow for the survival of genetically damaged cells and can lead to an increase in growth of lung cancer cells. However, when p53 reverts back to the wild-type state, the malignant phenotype of NSCLC can be prevented (14). $p16^{INK4A}$ is a gene product of the $p16^{INK4A}$-cyclin D1-CDK4-RB pathway which controls the G1 to S phase transition of the cell cycle (12).

$p16^{INK4A}$ typically arrests cells in the G1 phase, resulting in hypophosphorylation of RB, which is the active growth-suppressing form of RB. Inactivation of $p16^{INK4A}$ leads to a loss of controlled growth and NSCLC progression (15). K-*ras* partially encodes a member of the guanosine triphosphate binding protein family that regulates cell growth, differentiation and apoptosis (16). Mutation in this gene leads to dysregulation of these processes. Approximately 15 to 25% of patients with NSCLC have K-*ras* mutations (17).

1.1.3 Pancreatic Cancer

PDA has a characteristic pattern of genetic lesions that result in cancer development and progression (18). Similar to lung cancer, these lesions include mutations to K-*ras*, CDKN2A and TP53 (3). K-*ras* mutations are the first genetic changes detected in PDA progression, with the frequency increasing with disease progression (19). Although the specific pathways and influence of K-*ras* in PDA have not been identified, activating mutations to the *RAS*-family of oncogenes have been shown to induce proliferation, survival and invasion of pancreatic cancer cells (20). PDA overexpresses epidermal growth-factor (EGF) family ligands. These molecules are involved in an autocrine loop with *RAS*-family oncogenes (21) and may play a role in influencing cell proliferation. CDKN2A is a tumor-suppressor locus, located at 9q21 and encodes two tumor suppressors, INK4A and ARF. Deletion of 9q21 results in the loss of INK4A and ARF transcription and therefore disruption of the retinoblastoma (RB) and p53 tumor-suppressor pathways (22). Mutations of TP53 typically occur later in the progression of PDA and may reflect the function of TP53 in preventing malignant

progression (18). TP53 mutations are predictors of a poor survival rate of patients (23), possibly due to interactions between K-*ras* and CDKN2A.

1.1.4 Tumor Heterogeneity

Though tumor types vary in distinguishing characteristics, the majority of tumors share the common feature of variability among cancer cells within a single neoplastic lesion (24). Cancer cells can be distinguished one from another through a variety of characteristics including morphology, invasive and metastatic ability and sensitivity to pharmacologic agents (25). This intra-tumoral heterogeneity may be explained through a combination of the cancer stem cell hypothesis and the clonal evolution model (26). The cancer stem cell hypothesis states that the cancer-initiating cell is a transformed or mutated tissue stem cell. This altered tissue stem cell would retain the pivotal property of self-protection through use of a variety of multiple drug resistance transporters, while retaining canonical abilities for continuous self-renewal that define stem cells (27). The clonal evolution model suggests that cancer progresses through an evolutionary process driven by stepwise, somatic-cell mutations with sequential, sub-clonal selection (28). Combining the two theories together suggests that tumor heterogeneity arises through the sequential mutation of cells with the propensity of self-renewal at each step. What results is a collection of cells with differing collections of mutations determined by when the mutation occurred during the stepwise process.

The microenvironment of a tumor is heterogeneous as well, with different regions of the tumor having different densities of blood and lymphatic tissue, different numbers and types of infiltrating cells and different compositions of extracellular matrix (29).

Interactions of tumor cells with their microenvironment can shape malignant behavior and promote tumor progression (30). The primary tumor and its resulting metastases can become dramatically different during tumor progression, especially if the metastatic spread occurs early in tumor development. Additionally, this intra-tumoral heterogeneity can represent a challenge to therapeutic success since, as genetic diversity within a tumor increases, there would be a similar increase in the probability of the pre-existence of therapeutic resistant cell types. Furthermore, this therapeutic resistant populations would be selected for during treatment and could ultimately lead to the relapse of therapeutic resistant tumors (31).

1.1.5 Current Treatment Strategies

Standard of care for cancer patients includes surgical resection, chemotherapy and/or radiation therapy. In pancreatic cancer, only 5 to 25% of patients have an operable tumor. Median of survival from diagnosis is 8-12 months, and only 3-6 months in patients presenting with metastatic disease (32). Gemcitabine is currently the drug of choice for treatment of pancreatic cancer, with 5-Fluorouracil and capecitabine used in combination; however there is no significant benefit to these treatments in terms of longevity (33). Most NSCLC tumors are unresectable and treatment relies heavily on chemotherapy agents, including platinum-based therapy (34). Both doxorubicin and vincristine have been approved for treatment of PDA and NSCLC.

1.1.6 Nanomedicines

Nanomedicines consist of therapeutic agents encapsulated or conjugated to a nano-sized carriers with a size ranging from approximately 10 to 1000 nm. Many therapeutic agents for treatment of cancer have not been effective due to their limited ability to reach targeted tissues, combined with their cytotoxic effects on both malignant and normal cells (35). Nanomedicines were shown to be superior to their unencapsulated counterparts by not only limiting the damage to normal cells (36), but also by increasing accumulation of drug at the tumor site. This accumulation of nanomedicines occurs due to the enhanced permeation and retention (EPR) effect due to physiochemical features of the nanomedicines which include molecular size, biocompatibility, proper surface charge and the stability of the composing molecules (37). The EPR effect relies on the higher vascular density of tumors and the tendency of these vessels to be leaky or non-selectively permeable resulting from rapid and incomplete angiogenesis. Due to this leakiness, there is an increased opportunity for nanomedicines to escape from tumor blood vessels and accumulate in the tumor, especially in comparison to the less permeable blood vessels of normal tissues (38). The resulting accumulation of nanomedicines in tumor and neighboring cells by passive targeting is called the bystander effect (39). Relying completely on the EPR effect for drug delivery can lead to ineffective treatment due to different pore dimensions in the vasculature between tumor types, pore size changes between locations (primary *vs.* metastasis) and differences in vessel structure in a single tumor type (40).

1.1.7 Active Targeting

Active targeting has been studied as a method to improve the specificity and functionality of drug-loaded nanocarriers. Active targeting uses molecular recognition of a ligand-target nanocarrier by the counterpart receptor located in the cell membrane, microenvironment, cytoplasm, or nuclear envelope (41). A variety of ligands, including small molecules, peptides, aptamers, proteins and antibodies, are currently being studied for their use in targeting various nanocarriers (42,43). For example, a cyclic (RGDfE) conjugated nanomedicine with a magnetic core and mesoporous shell loaded with gemcitabine can target a pancreatic cancer cell line efficiently and specifically (44). For lung cancer, mutational hotspots have been mapped (45). This could lead to development of targeting ligands against these specific mutations through targeting of the normal and mutant proteins. Active targeting of the tumor stroma, including tumor endothelial cells, fibroblasts, mesenchymal cells and innate and adaptive immune cells, can modify the tumor microenvironment and make it difficult for tumor cells to grow (46).

While active targeting can address some of the limitations of passive accumulation, including specificity, there are still shortcoming to current methods. As discussed above, tumors are heterogeneous in nature. This heterogeneity can pose a problem when it comes to selecting an appropriate ligand for active targeting due to the variability of receptors expressed on tumor cells (47). A variety of receptors can be expressed not only between cells within a tumor, but also between cells in the primary tumor and related metastases. Due, in part, to tumor cell receptor heterogeneity, passive accumulation of drug may be more effective in treating metastases due to the limits of

specific targeting (48). However, by selecting ligands that act promiscuously with the ability to bind more than one receptor, the heterogeneity problem can be addressed.

1.2 Summary

It is widely accepted that tumors are extremely heterogeneous tissues, not only within the same tumor but across the disease and patient as a whole. This heterogeneity can be influenced by genetic changes, stage of progression, vascular pressure and many other factors. Due to this heterogeneity, identification of targeting ligands for nanoparticles designed to aid with diagnosis and treatment of cancers can be difficult. Work described here was desgined to advance a multi-target biopanning scheme for identification of ligands with pan-cancer binding abilities using landscape phage display technology. These promiscuous cancer binding landscape phage proteins have the potential to improve nanoparticle-based technology for identification and treatment of heterogeneous cancer cell populations.

Chapter 2:
Selection of Promiscuous Tumor Targeting Phage Proteins

2.1 Abstract

Because cancer remains one of the leading causes of human deaths, novel approaches with greater efficacy are urgently required for cancer treatment. Active targeting of chemotherapies to the site of pathology is one of the new approaches believed to have potential for clinical use. Targeting ligands, recruited from a variety of natural or selected molecules have been used successfully to modify currently used drugs and drug delivery systems to increase their efficacy. Cancer-specific targeting ligands for a variety of cancer cell lines have been identified previously using biopanning with phage display libraries, and their ligands have been used for targeting of nanomedicines. Tumor heterogeneity is a recognized problem hampering the successful use of targeted cancer treatments. In this work, using a novel selection scheme, promiscuous phage fusion proteins were identified with pan-cancer binding abilities, indicated by structural motifs comparable to those previously found in a variety of cancer types. Several phage fusion proteins were studied for their specificity to and selectivity for lung and pancreatic cancer cells. Phage displaying the fusion peptides GSLEEVSTL or GEFDELMTM were used to modify preformed, drug-loaded, liposomal doxorubicin. These preparations increased cytotoxicity up to 8.1-fold in several lung and pancreatic cancer cell lines when compared to unmodified liposomal doxorubicin. Taken together, data indicate that promiscuous phage proteins selected against two different cancer cell lines, as a model of cancer

heterogeneity, show potential as targeting ligands for treatment of heterogeneous tumors and their distant metastases.

2.2 Introduction

Cells within a tumor population can differ in organization, morphology, size, nuclear morphology and gene expression (11). The origins of this intra-tumor heterogeneity were proposed to be due to a combination of mechanisms explained by the cancer stem cell hypothesis and the clonal evolution model (26). This heterogeneity complicates cancer therapies that can alter tumor progression and increase the probability of enriching the tumor with pre-existing cells displaying treatment resistant phenotypes (31). While heterogeneity often occurs in the primary tumor, primary treatment options, which often include surgery, are not impacted severely by a heterogeneous phenotype. Tumor heterogeneity also occurs in metastatic lesions, which are typically inaccessible for resection and must be treated using chemo- or radiation therapy. Heterogeneity observed between the primary tumor and its metastases leads to a very complex and multifaceted disease that is difficult to treat with current therapeutic regimens.

Due to the difficulty in treating tumors using traditional tools, novel strategies based on newly developed nanotechnology are being used to increase the efficacy of treatments. Nanomedicines can be superior to non-encapsulated chemotherapeutic protocols due to their ability increase therapeutic index of chemotherapies through increasing the deposition at the tumor, while decreasing related side effects caused by the unencapsulated drugs. These benefits have been attributed, at least in part, the ability to engineered nanomedicines accumulate more specifically at the tumor. This is due, in

part, to the enhanced permeation and retention (EPR) effect. The EPR effect relies on the ability of nanomedicines to remain in circulation for longer periods of time, as well as passive accumulation in tumors *via* vascular defects commonly associated with rapidly forming blood vessels, characteristic of some cancer types. This allows for an increase in accumulation and retention of nanomedicines within the tumor microenvironment (49). Increased deposition is commonly achieved by altering certain physicochemical features of the nanomedicines (37). Vessels within a single tumor can vary in their permeability, resulting in inconsistent treatment accumulation (50). Thus, the passive accumulation of nanomedicines by the EPR effect can be highly variable between diseases and can result in inconsistent treatment efficacy both within and among patients with similar tumors.

It has been hypothesized that active targeting can be used to increase tumor-specific effects of passive accumulation while allowing for more even distribution of the therapeutic agent(s) and more effective treatment. Active targeting uses targeting moieties, such as antibodies or peptides, to direct nano-sized particles to specific disease-related receptors. Ideally, the actively targeted particle should be able to reach the target with minimal loss of treatment volume and limited toxic side effects (51). However, most actively targeted nanomedicines still require passive accumulation at the tumor *via* the EPR effect for to cell-specific targeting to occur. This is due primarily to the inability of commonly used nanoparticles to extravasate effectively through normal, non-leaky blood vessels (52). Another shortcoming of current active targeting strategies is the assumption that the targeted receptor will be expressed homogeneously on all targeted cells (47). Because of the tumor heterogeneity noted, a more promiscuous targeting strategy is required for successful treatment.

Bacteriophage libraries have been used to identify ligands specific to numerous targets including mammalian and bacterial cells, both *in vitro* and *in vivo* (53-55). The Ff class of filamentous bacteriophage have been used to display foreign peptides on the various phage proteins which in turn provides a vast source of ligands for targeting (56). The class Ff is made up of the phages fd, f1 and M13, with the virion filament formed by thousands of helically arranged copies of the major coat protein, pVIII and the ends are composed of two different pairs of proteins, pVII-pIX and pIII-pVI, all arranged around a single-stranded, circular DNA genome (57). The Ff bacteriophage infect Gram-negative bacteria via their F pili (58). This infection is mediated by the pIII protein, with the N-terminal domains binding to receptors on the pilus and the C-terminal domain facilitating virion uncoating and DNA entry into the bacterial cell cytoplasm (59). Pili that serve as receptors for filamentous bacteriophage share the ability to retract towards the surface of the bacterial cell, bringing the phage to the cell body. Previously it was thought this retraction was initiated by the bacteriophage binding to the pilus, however it has been recently shown that the F pili undergoes spontaneous extension and retraction cycles (60). As infection continues, the coat proteins of the bacteriophage are dissolved into the surface envelope of the bacteria cell and the uncoated ssDNA enters the cytoplasm (56).

Once in the cytoplasm, the phage replicate one strand at a time. The positive strain of the Ff bacteriophage ssDNA serves as a template to synthesize the negative strand. The positive ssDNA strand of the Ff phage genome is called the infective form (IF) and the dsDNA form is called the replicative form (RF), which serves as a template to synthesize the positive strand. The newly synthesized phage ssDNA is covered with dimers of pV, a phage-encoded ssDNA-binding protein, resulting in the DNA collapsing into a rod. The

packing signal, which is a hairpin loop, remains exposed and interacts with the assembly machinery on the inner surface of the bacteria cell (57). When the phage interacts with the this machinery, pVII and pIX are attached to the end of the virion, initiating assembly (61). The assembly machine is composed of an inner membrane ATPase channel and an outer membrane channel that the phage passes through (62). As the ssDNA passes through the membrane, the pV dimers dissociate and are replaced by pVIII. The virion is extruded from the bacteria cell membrane as it is assembled. Once the DNA is coated with pVIII, the minor coat proteins pVI and pIII are added to the end, triggering the release of the phage from the bacteria cell (63). Through this mechanism the progeny phage can be continuously produced and secreted from the bacteria cells without killing the host. However, due to the burden of phage production, division of infected bacteria cells occurs more slowly than normal (56).

Phage display libraries, which are collections of different bacteriophage that contain unique foreign DNA segments which correlates to the expression of the corresponding fusion peptides on the virion surface, have been created using a variety of vectors (64). These phage display libraries can have diversities ranging to upwards of 10^9 unique fusion peptides (65). First, fusion peptides were expressed on the minor protein pIII followed by expression on the major coat protein pVIII (56,66). Libraries utilizing a fusion peptide on pVIII are termed "landscape phage" due to the dramatic change in surface architecture caused by the insertion of the foreign sequences on the thousands of identical peptides on surface of the virion capsid. Specifically, f8 landscape phage display libraries are designed using derivatives of the filamentous bacteriophage vector, fd-tet, with random insertions within the gene encoding the pVIII major coat protein,

resulting in the random inserts being expressed in every copy at the N-terminal end of the pVIII major coat protein of the wild-type vector. In fd-tet-derived vectors random inserts are expressed in approximately 4,000 copies across the length of the phage particle (56,67). The f8/9 landscape phage display library, used in this work, consists of approximately 1.4 billion of phage variants composed of a variety of major coat proteins pVIII fused with foreign random 9-mer peptides with the common sequence

NH2-A**XXXXXXXXX**PAKAAFDSLQASATEYIGYAWAMVVVIVGATIGIKLFK KFTSKAS-COOH,

where X indicates random amino acids of the inserted fusion peptide (65).

Phage display has been extensively used for the generation of protein ligands that interact with surface receptors across a variety of sources (56). When compared to antibodies, filamentous phage and their isolated coat proteins maintain their target binding functionality after exposure to harsh environmental conditions, including high temperatures (68), which makes them intriguing candidates for use as targeting ligands. Phage and their isolated proteins can be produced efficiently and inexpensively in large quantities, which is advantageous in comparison to antibodies. A variety of platforms derived from protein products of phage display libraries have been developed for numerous diagnostic and therapeutic applications. Some of these platforms include targeted nanoparticles for gene delivery (69), MRI probes (70), probes for mapping of neoplastic and normal vasculature (71,72) as well as for cancer research including siRNA delivery (73), identification of binding peptides to various cancers (53-55,74,75), development of targeted nanorods for photothermal therapy (76), identification of ligands

for targeting of liposomes or micelles with therapeutic agents to a variety of cancer cell lines, including pancreatic, breast, prostate and malignant glial cells (54,77-80).

A number of cell surface receptors are uniquely or aberrantly overexpressed in neoplastic tissue. Identification of these receptors was enabled through the use of landscape phage display screening (54,55,75) and by use of other ligand libraries (53,81). However, most screening protocols are completed *in vitro* using a single cancer cell line and may not accurately depict the inherent heterogeneity of tumors *in vivo*. To address this issue we hypothesized that phage ligands selected from different cancer cell lines would demonstrate greater promiscuity in their binding capabilities to cancer cells within a single ligand. If so, this should increase the probability of interaction of targeting ligands and receptors within a heterogeneous tumor population as well as tumor metastases. Additionally, it was hypothesized that promiscuous pVIII major coat proteins isolated through a multi-target selection strategy could be used to modify preformed liposomal nanomedicines and increase the toxicity of these existing chemotherapies to a number of different cancer cell lines. To prove this novel concept, we used the previously characterized 9-mer landscape phage library, f8/9, as a source of ligands in an *in vitro* screen against lung and pancreatic cancer cell lines as a model of tumor heterogeneity. Numerous phage clones were identified as being specific to the two target cell lines. Additionally, several common structural motifs were identified during other phage biopanning (screening) experiments against other neoplastic cells. Results indicate that two of the selected phage ligands increased the efficacy of liposomal doxorubicin in several cancer cell lines in comparison to unmodified liposomes,

suggesting their potential applicability to treat heterogeneous cell populations with a single targeting ligand.

2.3 Materials and Methods

Cell Culture

Cell lines, PANC-1, Calu-3, A549 and MIA PaCa-2, were purchased from American Type Culture Collection (ATCC, Manassas, VA, USA) as frozen slugs. No additional cell line verification was performed. Cells were cultured in 25 cm^2 cell culture treated flasks (Corning, Corning, NY) and maintained in a humidified incubator at 37°C in 5% (v/v) CO_2 as described in the technical bulletins. Cells were subcultured when approximately 80% confluence was reached and reseeded at an approximate density of 4×10^4 cells/cm^2. The human lung adenocarcinoma cell line, Calu-3 (ATCC® HTB-55™), was cultured in ATCC-formulated Eagle's Minimal Essential Medium (EMEM) with 10% v/v defined fetal bovine serum (FBS, Hyclone, Thermo Fisher Scientific) and 1% v/v 100X antibiotic/antimycotic (Ab/Am) obtained from Thermo Fisher Scientific (Waltham, MA). The human pancreatic epithelioid carcinoma cell line, PANC-1 (ATCC® CRL-1469™), was cultured in ATCC-formulated Dulbecco's Modified Eagle's Medium (DMEM) with 10% v/v heat-inactivated FBS and 1% v/v Ab/Am. The human lung carcinoma cell line, A549 (ATCC® CCL-185) was cultured in ATCC-formulated Kaighn's Modification of Ham's F-12 Medium, with 10% v/v FBS and 1% Ab/Am. The human pancreatic carcinoma cell line, MIA PaCa-2 (ATCC® CRL-1420) was cultured in ATCC-formulated DMEM, with 10% v/v FBS, 2.5% v/v Horse Serum (ATCC) and 1% v/v Ab/Am. Primary human lung epithelial cells, Small Airway Epithelial (SAE) cells

(ATCC® PCS-301-010™) were cultured in ATCC-formulated Airway Epithelial Cell Basal Medium supplemented with the ATCC Small Airway Epithelial Cell Growth Kit and 1% v/v Ab/Am. Cell lines were grown on a 96-well plate (Corning) for all selectivity and cytotoxicity assays.

Reagents

Tween 20, glycine, Tris base, hydrochloric acid, sodium deoxycholate, EDTA, isopropanol and chloroform were purchased from Fisher Scientific (St. Louis, MO). Bovine serum albumin (BSA), 3-[93-Cholamidopropyl) dimethylammonio]-1-propanesulfonate (CHAPS), 3-(4,5-dimethylthiazol-2-yl)-2,5-diphenyltetrazolium bromide (MTT), sodium dodecyl sulfate (SDS) and Triton X-100 were purchased from Sigma Aldrich (Milwaukee, WI). 10X phosphate buffered saline (PBS) stock, Wheat Germ Agglutinin Alexa Fluor® 555 membrane stain, Goat Anti-Rabbit Alexa Fluor® 488 conjugated IgG and TOPRO-3 nuclear stain were purchased from Invitrogen (Carlsbad, CA). The Amicon Ultra-4 100 kDa centrifugal concentrators were purchased from Millipore (Billerica, MA). The *Taq* PCR master mix was purchased from Qiagen (Valencia, CA). Paraformaldehyde stock was purchased from Electron Microscopy Sciences (Hatfield, PA), Vecta Shield mounting medium was from Vector Laboratories, Inc. (Burlingame, CA) and 20X Tris buffered saline (TBS) stock was purchased from USB (Cleveland, OH). Liposomal doxorubicin (Lipodox), with 10.49 mg/mL lipid content composed of 2.21 mg/mL 1,2-distearoyl-sn-glycero-3-phosphoethanolamine-N-[amino(polyethylene glycol)-2000] (DSPE-PEG), 6.24 mg/mL 1,2-distearoyl-sn-glycero-3-phosphatidylcholine (DSPC) and 2.04 mg/mL cholesterol, was purchased from Sun

Pharmaceutical Ind. (Mumbai, Maharashtra, India). The polyclonal rabbit anti-phage IgG antibody was produced previously (82).

Phage display libraries

The f8/9 landscape phage library, which displays a 9-mer fusion peptide at the N-terminus of each copy of the pVIII major coat protein (66), was used as the input to screen against Calu-3 and PANC-1 cell lines to isolate clones that bind receptors common to both cell lines. All methods used for handling phage, including propagation, purification, titering, isolation and sequencing of phage clones have been described previously (83). The *Escherichia coli* strain K91BlueKan (Kan^r Hfr C thi lacZΔ M15 lac Y::mkh lacI^Q), which was used for propagation and titering of phage, was provided by George Smith (University of Missouri, Columbia).

Selection

The multibillion clone f8/9 phage library was used in a selection scheme similar to those previously described (55) with modifications biased to enrich the selected phage population for clones with more promiscuous binding abilities towards heterogeneous populations of different cancer cell lines. A total of three rounds of selection were performed from a portion of the parent library, with the first round of selection performed on a lung cancer cell line, Calu-3 and the remaining two rounds (2-3) performed on a pancreatic cancer cell line, PANC-1, as summarized in Figure 1A.

(A) Selection Against Lung Cancer Cells. An aliquot of the f8/9 phage library containing 1.2×10^{11} virions was incubated at room temperature for 1 hour with blocking buffer (0.5% w/v BSA in serum-free EMEM) in an empty 25 cm^2 cell culture flask to remove phage that bind non-specifically to plastic. The unbound phage were collected

and transferred to a cell culture flask that was incubated overnight with 10% serum to deplete the library of clones that strongly bind serum. Serum depletion was twice, for maximum efficiency in reducing undesired serum binding phages. The final depletion step was performed against phenotypically normal SAE cells at room temperature for one hour. The depleted f8/9 library was then added to a 25 cm^2 cell culture flask containing 90% confluent Calu-3 lung cancer cells and incubated at room temperature for 1 hour. After incubation, the cells were washed and phage was recovered as detailed in section C.

(B) Selection Against Pancreatic Cancer Cells. An aliquot of the amplified eluate phage library from the Calu-3 selection, containing 1×10^{11} virions was used as the input for the second round of selection against PANC-1 pancreatic cancer cells. The same protocol was used as described in section A with the exception that the cells were incubated at 37°C rather than room temperature to increase stringency and to better mimic physiological conditions. The eluate and lysate sublibrary fractions generated from the second round of selection were used as the input for the third round of selection with PANC-1 cells at 37°C to further enrich for phage clones associated with PANC-1 cells.

(C) *Washing and Sublibrary Generation.* After removing unbound phage, the flask was washed 10 times with 4 mL cold washing buffer (0.1% Tween 20 and 0.5% w/v BSA in serum-free medium, EMEM was used for the first round of selection and DMEM for the remaining rounds) for 5 minutes each to remove remaining weakly bound phage. The phage accumulated in the 10 washing portions were retained for titering with K91BlueKan *E. coli* cells. Cell surface-bound phage were recovered by incubating target cells with elution buffer (200 mM Glycine, pH2.2/ 0.1% w/v BSA) for 10 minutes on ice

then neutralized with 1M Tris-HCl, pH 9.1. The cells were then washed twice with 4 mL washing buffer and the washings were retained for tittering, which were termed Post Elution Wash 1 and 2 (labeled PEW1 and PEW2 respectively). The eluate fraction and PEW 1 and 2 from each round were concentrated together with Amicon Ultra-4, 100kDa centrifugal concentrators following the manufacturer's protocol (termed eluate fraction). Cancer cell penetrating phage virions were recovered by lysing the target cells. The cell monolayer was scraped from the flask in 5 mL of serum-free medium (EMEM for Calu-3 and DMEM for PANC-1) and added to a 15 mL conical tube (Corning). The cells were pelleted by centrifugation and the supernatant was removed but retained for titering. The pelleted cells were suspended in lysis buffer (2% w/v Sodium deoxycholate, 10 mM Tris, pH8.0, 2 mM EDTA) and the suspension was retained for titering and amplification. The combined eluate and post-elution wash fractions (surface bound phage) and lysate (cell penetrating phage) fractions were amplified in K91BluKan *E. coli* cells and purified by PEG/NaCl precipitation separately to be used during following selection procedures.

(D) Isolation of Individual Clones. Phage clones from the final round of selection were chosen at random for identification of the fusion major coat protein pVIII sequence through translation of the DNA sequences. Individual clones were gridded on NZY/Tet agar plates and incubated at 37°C overnight. The *gpVIII* sequence was amplified by PCR as described previously (83). The samples were sequenced by dye-terminator method at the Massachusetts General Hospital DNA Core (MGH DNA Core, Cambridge, MA, USA). All unique clones were propagated in 2 mL scale for further study. The full length sequence of the pVIII major coat protein is NH_2-A**XXXXXXXXXX**PAKAAFDSLQASATEYIGYAWAMVVVIVGATIGIKLFKKF

TSKAS-COOH (designated by the sequence of the fusion peptide at the N-terminus; XXXXXXXXX).

Computational Analysis

The identified *gpVIII* sequences from selected phage clones were translated to their corresponding pVIII protein sequences using the EditSeq program (DNASTAR, suite of molecular biology analysis programs, version 11, Madison, WI). Phage clones were analyzed to identify common structural motifs and grouped into families based on consensus motifs. Identified unique phage clones were analyzed for information content using the INFO tool found within the RELIC suite of statistical analysis for combinatorial peptide libraries programs (84). Additionally, the overall diversity of the pre- and post-selected f8/9 library was calculated using the AADIV tool found within the RELIC program suite. Identification of similar motifs identified after selection against other cancer cell lines or known cell surface receptors and the selected promiscuous f8/9 phage clones was completed using MimoDB (version 4.3, updated July 2014).

Specificity of Phage Clones

Unique phage clones were studied for their specificity towards Calu-3 and PANC-1 cells in comparison to SAE cells and serum as previously described (55). Briefly, each cell line (Calu-3, PANC-1 and SAE cells) was plated in triplicate at a density of 5.0×10^4 cells per well on a 96-well plate with the last 3 columns being only complete EMEM (EMEM supplemented with 10% FBS and 1% Ab/Am). After allowing the cells to attach and grow to confluence overnight, the cells were incubated with serum-free medium (EMEM for Calu-3, DMEM for PANC-1 and Airway Epithelial Cell Basal Medium for SAE cells) for one hour at room temperature to allow the cells to synchronize into arrest

at a G1 cell cycle. The medium was removed and cells were incubated with phage (10^6 cfu/well) in serum-free medium (EMEM for Calu-3, DMEM for PANC-1 and Airway Epithelial Cell Basal Medium for SAE cells) for 1 hour at 37°C. The unbound phage were carefully removed and cells were washed 8 times with 100 µL of washing buffer (0.1% Tween 20, 0.5% BSA in serum-free EMEM) for 5 minutes each. The cells were then lysed with lysis buffer (2.5% CHAPS, 0.5% BSA, in serum-free EMEM) for 10 minutes on a rocker. The solution containing the cell-interacting phage from the crude cell lysate was then titered in *E.coli* as described above. For control purposes, an unrelated phage with the fusion peptide VPEGAFSSD (85) was used. Phage recovery (yield) was calculated as the ratio of output phage over input phage:

$$\text{Percent Recovery (\%)} = \frac{\text{Phage}_{\text{Output}}}{\text{Phage}_{\text{Input}}} \times 100$$

Intracellular Fate of Phage Observed Through Immunofluorescence

The rate and localization of phage binding and penetration into the target cells was visualized using confocal immunofluorescence microscopy. Calu-3 and PANC-1 cells were seeded at a density of 5×10^5 cells/well were grown on four-well chamber slides (Lab-Tek II, Nalgene) overnight. The slides were incubated with 10^7 virions of phage diluted in serum free medium (EMEM for Calu-3 and DMEM for PANC-1 cells) for 4 hours. An additional slide without phage incubation was used as a control. After removal of unbound phage, slides were washed 3 times with 1X PBS for 5 minutes per wash at room temperature. Cells were fixed with 4% (v/v) paraformaldehyde for 15 minutes at room temperature and then washed as above. Cells were then treated with a Wheat Germ Agglutinin Alexa Fluor® 555 conjugate at a 1:200 dilution in blocking buffer (1% BSA in 1X PBS, pH 7.2) for 20 minutes to stain cellular membranes.

Following membrane staining, the cells were washed and permeabilized using 0.1% Triton X-100 in 1X PBS, pH 7.2 for 10 minutes at room temperature. Cells were then blocked with 1% BSA for 1 hour prior to the addition of a rabbit anti-phage IgG (1:500 dilution in blocking buffer) for 1 hour at room temperature. Subsequently, cells were washed and incubated with a 1:500 dilution of a goat anti-rabbit Alexa Fluor® 488 conjugated secondary antibody for 1 hour in blocking buffer, washed as above and the nuclei were labeled with a 1:200 dilution of TOPRO-3 in blocking buffer for 10 minutes. Finally, cells were washed, protected with Vecta Shield mounting medium and cover slipped prior to imaging. Cells were visualized with a C1 confocal microscope and images were captured using NIS Elements (ver. 4.20; Nikon Instruments).

Phage Protein Isolation

Selected phage fusion major coat proteins pVIII were isolated using the procedure outlined by Gillespie *et. al.* (86). Briefly, phage DNA was precipitated from whole phage by reconstituting phage in 1X TBS, pH 7.4 and diluting with isopropanol to a final concentration of 75% isopropanol. A portion of chloroform was added (30 µL) to promote complete dissolution of phage particles. The sample was thoroughly vortexed and centrifuged to allow the precipitated DNA to be separated from the solubilized pVIII protein. The concentration of the isolated pVIII protein was determined by UV-VIS spectroscopy and converted to concentration using the molar extinction coefficients predicted by the program Protean program (DNASTAR, ver. 11; Madison, WI).

Liposomal Doxorubicin Modification

Isolated fusion phage major coat proteins pVIII were mixed at a protein:lipid ratio of 1:200 with Lipodox (containing 2.0 mg/mL doxorubicin), vortexed, immediately

diluted with 1X TBS, pH 7.4 and were incubated overnight at 37°C with gentle rotation. Samples were then purified using 100K NanoSep centrifugal devices (Pall life Sciences) and washed with 1X PBS, pH 7.2, to allow for buffer exchange and removal of free doxorubicin. Purified samples were stored at 4°C until further analysis and use.

Characterization of Phage Protein-Modified Nanomedicines

Major coat protein pVIII incorporation into the liposomes was determined using Western blot as previously described (55). The zeta potential and size distribution of unmodified and modified particles were measured by dynamic light scattering in 10 mM Tris-HCl, pH 8.0 using a Malvern ZetaSizer ZS90 (Malvern instruments, Ltd., Worcestershire, UK). The concentration of doxorubicin in the protein-modified liposomes was measured using UV-VIS spectrophotometry. Briefly, encapsulated doxorubicin was released from liposomes using 2% Trition-X-100 and the absorbance was measured at 490 nm on a BioTek Synergy H1 plate reader (BioTek Instruments, Inc., Winooski, VT). The concentration of doxorubicin for the protein-modified liposomes was calculated based on a standard curve of unmodified Lipodox.

Cell Viability of Phage Protein-Modified Nanomedicines

Cell growth was evaluated as described previously (54). Briefly, target cells were seeded at a density of 5×10^3 cells/well in a 96 well plate. The cells were incubated overnight at 37°C with 5% CO_2 in a humidified cell culture incubator. 5-fold dilutions were used for treatments, ranging either from 200 µg/mL to 0.064 µg/mL or from 100 µg/mL to 0.032 µg/mL, depending on the starting concentration of the protein modified and unmodified Lipodox samples. Treatment portions were diluted in complete medium and applied to the cells for 18 hours at 37°C with 5% CO_2 in a humidified cell culture

incubator. The solutions were aspirated and replaced with complete medium for 24 hours at 37°C with 5% CO_2 in a humidified cell culture incubator. The medium was then removed and replaced with 0.45 mg/mL MTT, diluted in phenol red-free MEM, 4 hours at 37°C with 5% CO_2 in a humidified cell culture incubator. 10% SDS in 0.01 N HCl was added and incubated overnight at 37°C with 5% CO_2 in a humidified cell culture incubator. The plate was read at 570nm on a Synergy H1 plate reader (BioTek) and cell viability was calculated based on untreated cells:

$$\text{Viable cells } (\%) = \left(\frac{\text{Abs}_{\text{treated cells}}}{\text{Abs}_{\text{untreated cells}}}\right) \times 100$$

Additionally, cell viability was confirmed through visual inspection of the cells after treatment (data not shown).

Statistics

Statistical analysis was performed using the JMP 11 (SAS Institute, Cary, NC). Analysis of phage binding was completed using a paired Student's T-test with $P<0.05$ as accepted as statistically significant. Data for phage specificity and cytotoxicity were subjected to analyses of variance using a Tukey-Kramer analysis, with $P<0.05$ accepted as statistically significant. Data from all experiments are shown as mean ± standard deviation (SD).

2.4 Results

Due to the heterogeneity commonly observed within tumors, targeting of specific receptors that are effective in the entire tumor cell population has proven difficult. Additionally, after the primary tumor has metastasized to distant locations, a new set of receptors that are specific to the metastatic lesions also needs to be considered. To

identify promiscuous ligands with the ability to interact with receptors common to different cancer cells, a landscape phage display library, displaying a randomized 9-mer fusion peptide on the pVIII major coat protein of the fd-tet phage vector, was screened against a representative lung and pancreatic cancer cell lines as a model of tumor heterogeneity through three subsequent rounds of selection (Figure 1A).

To ensure identified phage interact primarily with the targets unique to cancer cells, the library was first depleted against plastic, cell culture medium containing serum and phenotypically normal cells. The depleted library was then incubated with lung cancer cells (Calu-3) at room temperature to enrich for phage interacting with a variety of surface receptors. Phage clones binding the surface of the cell were eluted and washed twice with washing buffer to release cell surface and cytoplasmic phage. These fractions were combined to prepare the eluate fraction sublibrary. Cells were then lysed to collect membrane-bound, cell internalizing phage and amplified as the lysate library fraction.

Following recovery of phage binding Calu-3 cells, a portion of the resulting eluate library fraction was then incubated with a pancreatic cancer cell line (PANC-1) to broaden the promiscuity of the phage binding cancer receptors. Additionally, the temperature during phage incubation was increased from 20°C to 37°C to allow more phage to be recovered from the lysate library fraction due to an increase in active cell transport mechanisms. Selection was performed with PANC-1 cells as the target cell line for two additional rounds, with the second round of selection using the output libraries from the previous round of selection against PANC-1 cells, for a total of three rounds. The eluate input for the third round of selection consisted of the eluate sublibraries, (eluate-eluate and eluate-lysate) as well as the eluate portion of the lysate sublibrary

(lysate-eluate) to better identify cell penetrating phage in comparison to cell surface binding phage. Through each successive round of selection, there was an increase in the total number of phage recovered in the eluate and lysate fractions (Figure 1B). The total yield of phage recovered per round of selection is calculated by dividing the phage output following each round of selection by the total number of input particles as follows:

$$\text{Total Yield (\%)} = \left(\frac{\text{Phage}_{\text{Output}}}{\text{Phage}_{\text{Input}}} \right) \times 100$$

The resulting increase in phage recovered in each of these fractions can be attributed to an enrichment of cancer cell-specific binding or cell-penetrating phage clones. This enrichment occurs through not only removing phage that bind plastic, serum and non-neoplastic cells, but also through repeated rounds of incubation and propagation of the recovered clones with the target cells. Phage that bind cancer cell receptors with greater affinity than clones with lower affinity, dominate after extensive washes and elution prior to their amplification. Remarkably, we observed an increase in overall phage yield after each subsequent round of selection, which was performed in PANC-1 cells versus Calu-3 cells. We hypothesize that this increase is due to the recovery of phage able to bind both populations of cancer cells.

After the third round of selection, 200 phage clones (100 each from the eluate and lysate output libraries) were randomly chosen for identification of the DNA sequence encoding for the selected fusion coat protein. The DNA sequence of fusion gene *gpVIII* was amplified using PCR and sequenced. Analysis of the recovered clones yielded a total of 87 unique clones, representing several different families based on structurally conserved portions of the resulting peptide motifs (Table 1). Clones that did not reveal a shared motif were grouped into an "orphans" family for classification. Further analysis

of each of the families showed that several recovered clones contained more than one structurally conserved motif. It is speculated that the appearance of two distinct functional domains in the protein is due to enrichment of certain structural motifs during the first round of selection against lung cancer cells with these clones persisting through all following rounds of selection, while a secondary motif can also be selected against pancreatic cancer cells from the primary semi-random sublibraries. For example, we suggest that the large DGR family was selected during the first round of selection against lung cancer cells and the secondary motif that was revealed in several of these clones resulted from the subsequent enrichment during the second and third rounds of screening of semi-random sublibrary DGRXXXXXX election against pancreatic cancer cells.

The selected promiscuous phage clones were compared to the MimoDB database to identify similar motifs identified through other biopanning experiments with cancer cells and elucidate possible targets (Supplemental Table 1). One hundred and ten similar motifs were found from various biopanning experiments using different targets cells such as prostate, ovarian, bladder, skin, breast and colon cancers as well as cancer specific integrins and estrogen receptors. There were several clones containing large consensus sequences, exemplified by the phage clone AEYGESVNA. This clone was also selected from biopanning experiments with prostate cancer cells. We also identified the structurally conserved VSTL family, which was selected from previous biopanning experiments using breast and prostate cancers in addition to the lung and pancreatic cancer cell lines explored in this study (Table 2).

A statistical analysis of the promiscuous phage clones was performed using the RELIC suite of programs, which was specifically developed to study combinatorial

peptide libraries. Information content is used to compare the probability of an amino acid occurring randomly in the parent library in comparison to the amino acid being present following a biopanning experiment. A higher information content clone is assumed to have a lower probability to occur randomly due to an increase in underrepresented amino acids in comparison to the unselected library. This is thought to occur during selection, which creates a selective pressure to maintain the underrepresented amino acids. The total information content associated with the final promiscuously selected library was determined and compare with the initial library. All 87 unique clones were analyzed as representative of the output library for generation of information content in comparison to 64 random clones that are representative of the primary f8/9 library (Figure 1C). An increase in the higher information clones was observed following sublibrary generation of promiscuous cancer cell-binding clones (black line) in comparison to the primary library (gray line) as was hypothesized. Identified clones with higher information content were phage clones with the following fusion peptides: EVNVEEINL, EVSVEEINL, EDFAEIMQA and AEYGESVNA, which displayed higher binding to at least one of the target cell lines. This suggests that the selected promiscuous cancer cell-binding population is enriched for phage that can bind lung and pancreatic cancer.

Selectivity of Phage towards Pancreatic and Lung Cancer Cells

To determine the specificity of the selected phage, 87 unique clones were screened against the target cell line, PANC-1 and serum. The resulting yield of each phage for both targets was calculated as described previously. The top 20 clones were chosen based on the highest recovery of phage binding PANC-1 cells and the largest ratio of yields between PANC-1 and serum (Figure 2A). The goal of this step was to eliminate

slow growing, low binding, or otherwise inefficient clones from the list of clones to be used for the further study.

The identified clones were then screened for their selectivity towards the target cells, PANC-1 and Calu-3, in comparison to the non-target cell line, SAE and serum. The results from selectivity screening demonstrated that clones identified following a promiscuous selection scheme show a higher selectivity to the two different types of cancer cells and a greater specificity compared to phenotypically normal cells and serum (Figure 2B). Based on cumulative results of both binding assays with PANC-1 and Calu-3 and the minimal binding observed with the phenotypically normal lung cells, two of the top identified clones were GSLEEVSTL and GEFDELMTM. The GSLEEVSTL clone displayed a recovered phage yield of 0.068% in the PANC-1 cell line and 0.056% in the Calu-3 cell line. Compared to the unrelated targets, there was a significant difference observed ($P \leq 0.0001$ for both cell lines compared to SAE and 0.0003 and 0.0017 respectively for serum), suggesting this phage has a higher affinity to the target cells. Similarly, the GEFDELMTM clone displayed a recovered phage yield of 0.041% in the PANC-1 cell line and 0.10% in the Calu-3 cell line. Compared to the phenotypically normal cells, there was a statistically significant difference observed ($P = 0.0003$ and <0.0001, respectively), indicating this phage has a higher affinity to the target cells. There was a statistically significant difference observed between the Calu-3 cell line and serum binding ($P<0.0001$), however not for PANC-1 ($P = 0.0385$). Additionally, when looking at phage clones that bound either cell line strongly while still having an affinity for the other the top clones include DHVWAEGDS ($P <0.0001$ and 0.0016 for Calu-3 versus SAE and Serum, respectively) and DPNWEATVG ($P <0.0001$ for Calu-3 and

both SAE and Serum) for Calu-3 and AEYGESVNA (P= 0.0105 for PANC-1 and SAE) for PANC-1. These 5 clones, which display higher selectivity and specificity to the target cells as shown from these experiments, were studied further for their cell-specific interactions and subcellular partitioning using confocal immunofluorescence microscopy.

Intracellular Fate of Phage in Target Cancer Cells

Knowledge of the relative amount of phage that penetrate the tumor and bind to tumor components, along with identification of a subcellular location where phage accumulate, is important for consideration of the cancer cell-specific phage as a potential drug delivery vehicle and/or imaging reagent. Data on the rate and intracellular location of phage accumulation can also be valuable in selecting phage clones for targeting specific regions of the cell such as the nucleus or mitochondria. To study the intracellular fate of the selected clones, each phage was incubated with the target cells separately on a chamber slide for 4 hours at 37°C. After the unbound phage were removed, the cells were fixed with paraformaldehyde and permeabilized with Triton X-100. Phage and subcellular compartments were labeled and identified using antibodies specific for phage, cell membranes and nucleus that were each conjugated with a different fluorophore. An additional unrelated phage, VPEGAFSSD, was used as a negative control. After 4 hours of incubation, specific accumulation of the selected phage in both target cell lines was observed in comparison to the negative control. Phage bearing the fusion peptides GSLEEVSTL, GEFDELMTM and DHVWAEGDS showed the best cytoplasmic accumulation (Figure 3A). Additionally, these phage accumulated in the perinuclear space, suggesting a potential for their use in imaging and/or drug delivery. Nuclear penetration was observed for phage bearing the fusion peptides GSLEEVSTL (Figure

3B) and GEFDELMTM (data not shown). Due to the ability of these phage clones to be internalized rapidly within 4 hours and accumulation in/around the nucleus, it is hypothesized that they may be ideal candidates for use in the generation of tumor-targeted nanomedicines.

Modification of the Preformed Doxorubicin-loaded Liposomes

Tumor targeted variants of Lipodox (liposomal doxorubicin, containing 2 mg/mL doxorubicin) were obtained by fusion with the isolated pVIII fusion coat proteins bearing peptides GSLEEVSTL and GEFDELMTM, as previously described (86). Phage proteins were detected by Western blot following modification and purification of the phage protein-modified Lipodox samples (Figure 4A) in comparison with control protein samples. Additionally, we observed minimal changes in the relative surface charge and size distribution of the phage protein-modified Lipodox preparations (Table 3). There were 6.7 nm and 7.5 nm increases in size of the GSLEEVSTL and GEFDELMTM modified Lipodox, as well as a 0.4 mV increase and 1.2 mV decrease in the zeta potential respectively, which were determined not to be physiologically relevant in the biological system being studied. The majority of the initial doxorubicin input was retained after protein insertion (~60-85% recovery; Table 3).

Cytotoxicity of Phage Protein-Modified Lipodox

To determine if introduction of cancer cell-specific phage proteins can increase the cytotoxicity of Lipodox, the target cells Calu-3 and PANC-1, as well as A549 and MIA PaCa-2 cells, which are more drug sensitive than their respective counterparts, were incubated with various concentrations of phage protein-modified Lipodox in comparison to unmodified Lipodox for a 18 hour treatment. Lipodox modified with phage protein

GSLEEVSTL decreased PANC-1 cell viability at 40 and 8 µg/mL (P <0.0001 and 0.0026, respectively), Calu-3 cell viability at 200, 40 and 8 µg/mL (P= 0.0012, 0.0072 and 0.0043, respectively) and A549 cell viability at 200 and 40 µg/mL (P= 0.0015 and <0.0001, respectively) (Figure 5A). The drug sensitive pancreatic cancer cell line, Mia-PaCa2, was not studied with this preparation. GSLEEVSTL phage protein-modified Lipodox increased in cytotoxicity towards PANC-1, Calu-3 and A549 cells in comparison to unmodified Lipodox. This preparation showed a 2.4±0.9, 2.3±0.1 and 8.1±1.9 fold decrease in cell viability in PANC-1, Calu-3 and A549 cells respectively at a doxorubicin concentration of 200 µg/mL. Additionally, a 2.1±0.8 and 2.0±0.3 fold decrease in cell viability was observed in Calu-3 cells treated with GSLEEVSTL phage protein-modified Lipodox at 40 and 8 µg/mL of doxorubicin and a 3.4±1.4 fold decrease in cell viability of PANC-1 cells treated with GSLEEVSTL phage protein-modified Lipodox at 8 µg/mL of doxorubicin. These data suggest that phage protein-modified Lipodox is effective at increasing cytotoxicity of the untargeted nanomedicine at higher drug concentrations.

GEFDELMTM phage protein-modified Lipodox decreased PANC-1 cell viability at 20 and 4 µg/mL (P= 0.0003 and <0.0001, respectively**)**, Calu-3 cell viability at 100, 4 and 0.16 µg/mL (P=0.0068, <0.0001 and <0.0001, respectively), A549 cell viability at 100 and 20 µg/mL (P <0.0001, respectively) and Mia-PaCa2 cell viability at 100 µg/mL (P= 0.0008**)** (Figure 5B). GEFDELMTM phage protein-modified Lipodox showed a 2.4 ± 0.1 and 2.4 ± 0.2 fold decrease in cell viability in A549 and Mia-PaCa2 cell at a 100 µg/mL doxorubicin concentration. These results indicate that GSLEEVSTL phage protein-modified Lipodox and GEFDELMTM phage protein-modified Lipodox are more

effective at decreasing cell viability than unmodified Lipodox. Since two different cell types of both lung (Calu-3 and A549) and pancreatic cancer (PANC-1 and MIA PaCa-2) displayed decrease cell viability when treated with the protein modified Lipodox, these ligands may act similarly in targeting heterogeneous populations of tumors.

2.5 Discussion

Numerous targeted nanomedicines are currently being studied for efficacy in animal models and clinical trials for both pancreatic (87) and lung cancer (88). However, few drug preparations address the issue of cellular heterogeneity of both primary tumors and their resulting metastases. In this study several phage ligands that can be used to target both pancreatic and lung cancer cell populations specifically over phenotypically normal cells and serum, were identified. Given that these ligands display activity in cell lines against which they were selected (Calu-3 and PANC-1) as well as for different cell lines generated from the same diseases (A549 and MIA PaCa-2) when combined with similar motifs that were found to be specific for a plethora of cancer types (Supplemental Table 1), these ligands could be ideal for targeting a heterogeneous population of cancer cells. Studying cytotoxic effects of targeted therapeutics in drug-sensitive and insensitive cell lines provides a model system for evaluation of heterogeneous drug sensitivities reported in clinically observed tumors (31). This further supports the use of these ligands for targeting of heterogeneous cancer cell populations.

The phage selection scheme and results presented here enable identification of ligands with different presumed mechanisms of interaction with two different target cells. In the first example, single ligands were identified that can bind many different cell types,

presumably through interactions with the identified motif and a common surface receptor. In the second example, a single ligand was identified that contains more than one targeting motif. A combination of these two ligands may have applications for drug delivery and/or tumor imaging. If the first motif in the ligand is a cancer binding ligand, as demonstrated for the $\alpha_V\beta_5$ integrin-binding DGR motif (89), the second motif may be used to further enhance binding to each cell type after initial binding, which may only occur when the second motif is brought closer to its receptor by consequence of the first interaction. Of course, more than two binding motifs may be present in the selected ligands. This would explain the ability of the selected ligands to bind various cell lines derived from lung and pancreatic tumors.

Protein ligands identified through the promiscuous selection scheme employed here, could be used for modification of different nanomedicines, including liposomal and micellar scaffolds, nanorods and siRNA (73,76,90,91). Phage proteins specific for a desired target can be used to modify pre-formed, drug-loaded nanoparticles to target them specifically and increase to the activity of unmodified nanoparticles. These phage protein-targeted particles can be explored not only as chemotherapeutics, but also as diagnostic agents for earlier cancer detection, and for improved delivery of contrast agents and dyes used during tumor evaluation and resection (92). By using the promiscuous phage proteins identified here, visualization and treatment of metastasis may also be possible.

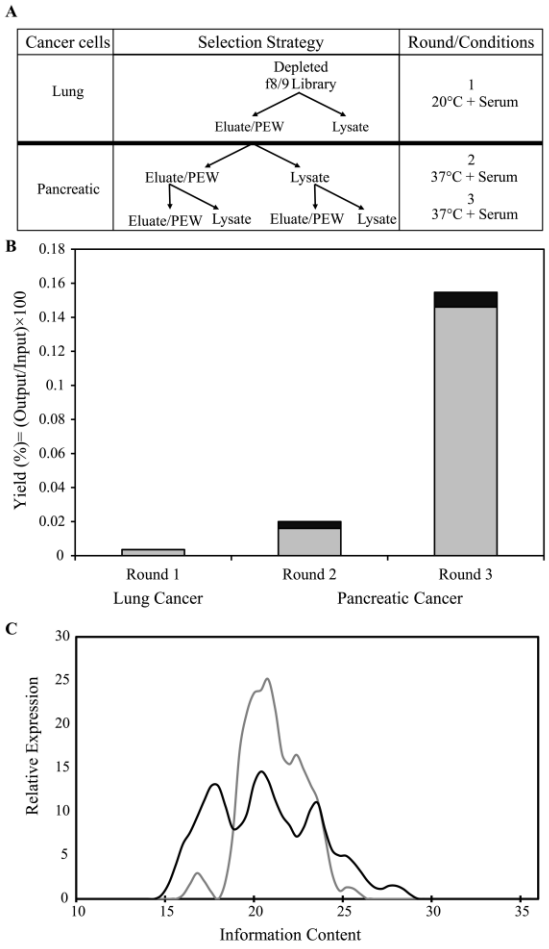

Figure 1: Promiscuous Phage Display Selection. (A) Selection strategy utilizing both lung and pancreatic cancer cells produces the Eluate-Eluate, Eluate-Lysate, Lysate-Eluate and Lysate-Lysate sub-libraries after each round of selection. The output for each round of selection is indicated by an arrow pointing from the input. The cell type and experimental conditions for each round of selection is shown at the right of the panel. (**B)** The total phage yield after each round of selection was calculated for both the eluate (gray bars) and lysate (black bars) fractions for comparison to other rounds of selection. **(C)** Histogram of the information content of the sublibrary of phage clones enriched with promiscuous cancer cell-binding (black line) compared to the parent f8/9 library (gray line).

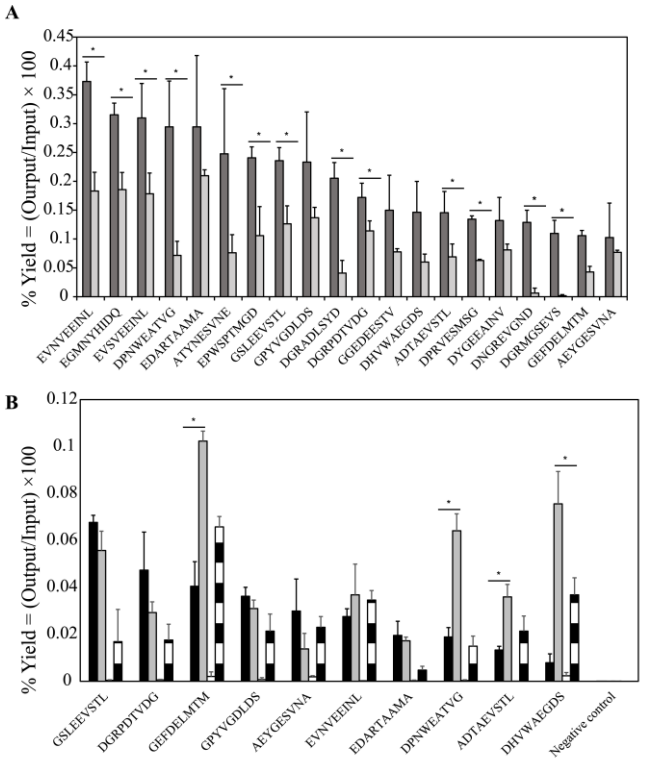

Figure 2: Selectivity and Specificity Assays of Phage Interactions with Target Cells. **(A)** Representative selectivity assay of phage clones interacting with either pancreatic cancer cells (dark bars) or medium containing 10% FBS (light bars). Data are represented as the mean phage yield ± standard deviation (SD). * indicates a *P*-value < 0.05, when comparing paired output yields of phage interacting with PANC-1 compared to serum. (**B)** Representative specificity assay of the selected phage clones were studied against pancreatic cancer cells (black bars), lung cancer cells (gray bars), normal lung cells (white bars) and serum (striped bars). The top nine clones were chosen based on either high binding to the pancreatic cancer and/or lung cancer cells or those clones with high target-to-serum ratios. VPEGAFSSD was included as a negative control. Data are represented as the mean phage yield ± standard deviation (SD). * indicates a *P*-value < 0.05, comparing paired output yields.

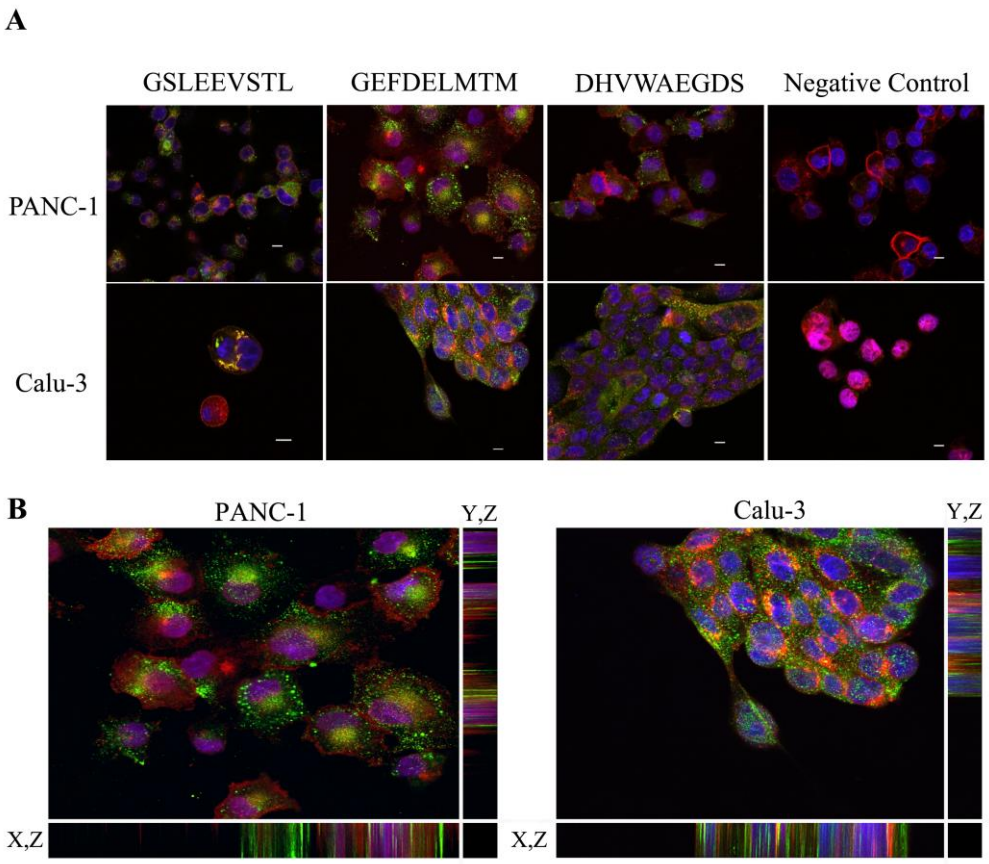

Figure 3: Intracellular Accumulation and Fate of Cancer-Specific Phage. (A) Intracellular fate of isolated phage clones in PANC-1 and Calu-3 cells. Cancer cells were incubated with 10^7 virions of each corresponding phage for 4 hours and visualized using confocal immunofluorescence microscopy. Phage were visualized with an Alexa Fluor® 488-conjugated anti-fd IgG (green), membranes with a Wheat Germ Agglutinin-Alexa Flour® 555 conjugate (red) and nuclei with TOPRO-3 (blue). All scale bars are 10 µm. **(B)** Intracellular accumulation of phage clone GSLEEVSTL. Orthogonal slices of the GSLEEVSTL clone after 4 hour incubation with both PANC-1 and Calu-3 cells. Phage were visualized with an Alexa Fluor® 488-conjuated anti-fd IgG (green), membranes with a Wheat Germ Agglutinin-Alexa Flour® 555 conjugate (red) and nuclei with TOPRO-3 (blue).

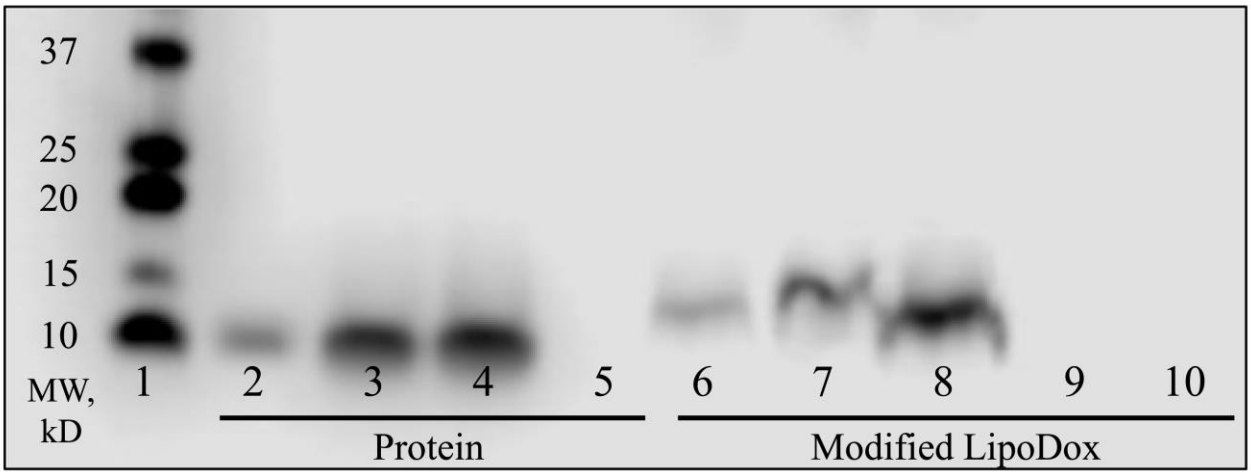

Figure 4: Physicochemical Characterization of Phage Protein-Modified Lipodox. Phage protein presence assayed by Western Blot. (1) Marker (2) VNGRAEAP protein (3) EPSQSWSM protein (4) GSLEEVSTL protein (5) Mock sample control (6) VNGRAEAP phage protein-modified Lipodox (7) EPSQSWSM phage protein-modified Lipodox (8) GSLEEVSTL phage protein-modified Lipodox (9) Mock Lipodox sample control (10) Unmodified Lipodox.

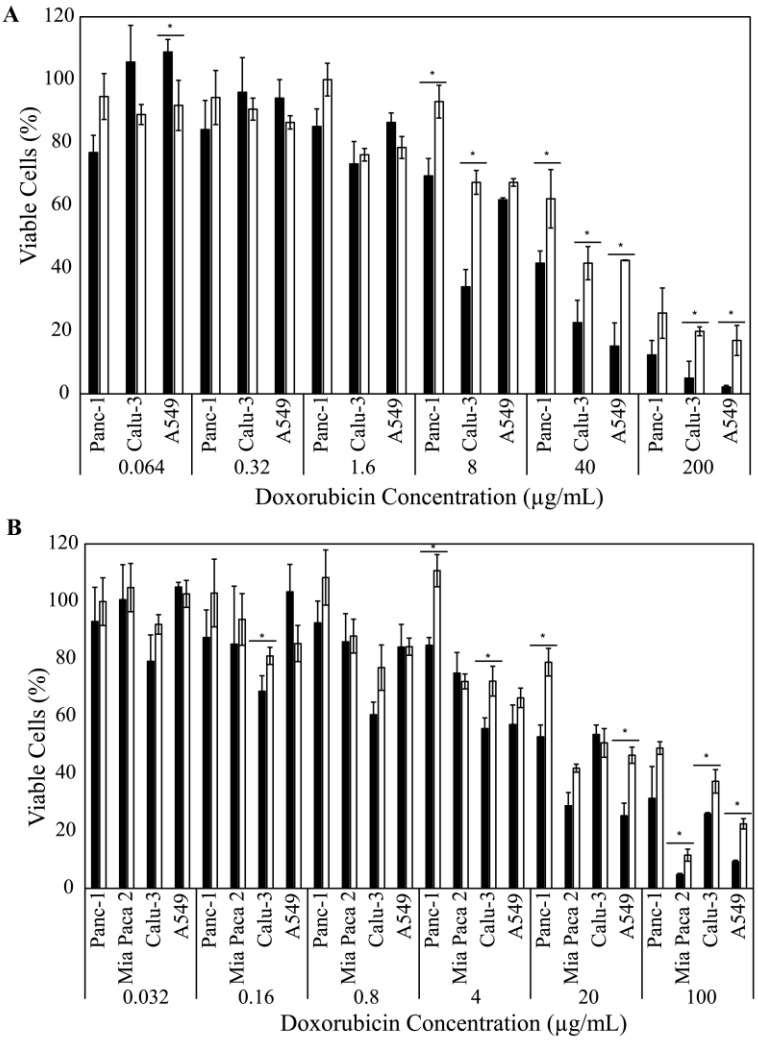

Figure 5: Cytotoxicity of Phage Protein-Modified Lipodox Preparations. (A) Cell viability as determined by MTT assay of GSLEEVSTL phage protein-modified Lipodox (black bars) compared to unmodified Lipodox (white bars) in several relevant cell lines. Percent viability was calculated by comparison of treated cells to untreated control cells, which were determined as 100% viable. * denotes a *P*-value < 0.05. (**B)** Cell viability as determined by MTT assay of GEFDELMTM phage protein-modified Lipodox (black bars) compared to unmodified Lipodox (white bars) in several relevant cell lines. Percent viability was calculated by comparison of treated cells to untreated control cells, which were determined as 100% viable. * denotes a *P*-value < 0.05.

AEV-TL	*DGR*	*DHV*	*EFD*	*EVT*	*GSL-E-STL*	*PEV*	*SVD*	*WSP---D*
ADT**AEVSTL**	**DGR**GYSSED	DGRPP**DHV**D	ESTRGL**EFD**	DPLA**EVT**TL	**GSL**A**E**T**STL**	GSD**PEV**VHL	GSA**SVD**MDM	EP**WSP**TMG**D**
DPL**AEVTTL**	**DGR**HLDQVD	**DHV**WAEGDS	G**EFD**ELMTM	EYAMR**EVT**E	**GSL**E**E**V**STL**	VGWS**PEV**PD	VQAFDD**SVD**	VG**WSP**EVP**D**
AFD	**DGR**ADLSYD	*DYS*	*ELVS*	*FDP*	*GTG*	*PGD*	*VDG*	*YGE*
AFDPDLHLN	**DGR**AYDVNE	AFGED**DYS**D	DYNP**ELVS**L	A**FDP**DLHLN	DELILV**GTG**	AF**PGD**ESDT	DGRFG**VDG**S	AE**YGE**SVNA
VQ**AFD**DSVD	A**DGR**DHYSD	E**DYS**ELVSQ	SDYS**ELVS**Q	VT**FDP**YDNN	DGRDG**GTG**S	GWGT**PGD**VD	DGRPDT**VDG**	D**YGE**EAINV
AEI	**DGR**DGGTGS	*ED-SEL*	*EPG(MD)*	*GDE*	*GVD*	*RAD*	**VDG**RLGDEH	*YNE*
EDF**AEI**MQA	**DGR**DHSGQD	**ED**I**SEL**NTL	ATG**EPGMD**A	AFP**GDE**SDT	DGRF**GVD**GS	DG**RAD**LSYD	**VDG**RMGDMG	AT**YNE**SVNE
GNM**AEI**TSL	**DGR**FGVDGS	**ED**Y**SEL**VSQ	VAVS**EPGMD**	DGRSIV**GDE**	VDWSTD**GVD**	VGIDEQ**RAD**	*VDW*	DGRMTV**YNE**
ASV	**DGR**FSDMPT	*EEA*	VY**EPG**LGTD	DVDGRL**GDE**	*GYSSE*	*REV*	**VDW**DNVSES	*Orphans*
GS**ASV**DMDM	**DGR**MGSEVS	AVGS**EEA**LL	*ESD*	*GDD*	DGR**GYSSE**D	DNG**REV**GND	**VDW**STDGVD	AVHDQDYDS
GSFSE**ASV**S	**DGR**MTVYNE	DYG**EEA**INV	AFPGD**ESD**T	DGRMVM**GDD**	**GYSSE**HLID	EYAM**REV**TE	*VEE(INL)*	DAASHNAED
AVG	**DGR**MVMGDD	*EEG-YIAA*	DGRSVM**ESD**	VLR**GDD**MNN	*G---E-STV*	*SEE*	EVN**VEEINL**	DNPWGLQPD
AVGSEEALL	V**DGR**MGDMG	G**EEG**E**YIAA**	*EST*	*GED*	**G**GED**E**E**STV**	AVG**SEE**ALL	EVS**VEEINL**	DPNWEATVG
GDYTE**AVG**A	**DGR**PDTVDG	V**EEGGYIAA**	**EST**RGLEFD	AF**GED**DYSD	**G**RME**E**V**STV**	VSYLE**SEE**S	**VEE**GGYIAA	DPRVESMSG
A-G-D-YSD	**DGR**PPDHVD	*EES*	GGEDE**EST**V	G**GED**EESTV	*LAE--TL*	*SES*	*VGD*	EDARTAAMA
AD**G**R**D**H**YSD**	**DGR**RDVADD	GGED**EES**TV	*E(V/T)S(TL)*	VIYPGV**GED**	DP**LAE**VT**TL**	DHYSS**SES**	DGRSI**VGD**E	EGMNYHIDQ
AF**G**E**D**D**YSD**	**DGR**RGEETD	VSYLES**EES**	ADTA**EVSTL**	*GEE*	GS**LAE**TS**TL**	VDWDNV**SES**	GPY**VGD**LDS	EHGNIEGNN
A---ESVN	**DGR**SIVGDE	*(E)EVST(L)*	ASME**EVSTL**	DGRR**GEE**TD	*MEEVST*	*SME*	**VGD**AGHSME	ESWGQGIPD
AEYG**ESVN**A	**DGR**SVMESD	ADTA**EVSTL**	DGRMGS**EVS**	DY**GEE**AINV	AS**MEEVST**L	A**SME**EVSTL	*VNE*	GYGFNQDQT
ATYN**ESVN**E	**DGR**YIGDND	ASM**EEVSTL**	EYDK**ETSTL**	**GEE**GEYIAA	GR**MEEVST**V	VGDAGH**SME**	ATYNES**VNE**	GYPIGGDTT
DEL	**DGR**YQDLPD	GRM**EEVST**V	GRME**EVST**V	*GSE*	*MGD*	*SSE*	DGRAYD**VNE**	RVPGSYSID
DELILVGTG	V**DGR**LGDEH	GSL**EEVSTL**	GSLA**ETSTL**	AV**GSE**EALL	DGRMV**MGD**D	DGRGY**SSE**D	*VSE*	VTLWEPDSD
GEF**DEL**MTM	V**DGR**MGDMG			DGRM**GSE**VS	EPQSPT**MGD**	DHYS**SSE**S	VA**VSE**PGMD	
					VDGR**MGD**MG	GY**SSE**HLID	VDWDN**VSE**S	

Table 1: Analysis of Identified Phage Clone Motifs. Sequenced phage clones were analyzed for similar structural motifs/families after the third round of selection and are shown in bold. Clones without an identified family are termed “orphans”.

Promiscuous Peptide[a]	Motif-containing peptides from other selected peptides	Target/Reference
AEYGESVNA	**AEYGES**G**NA**	Prostate Cancer (75)
	AEYGESVLI	Prostate Cancer (75)
	AEYGESVNA	Prostate Cancer (75)
	AEYGERG**NA**	Prostate Cancer (75)
DHVWAEGDS	GPN**WAEGDS**	Prostate Cancer (75)
DYNPELVSL	NHTT**EL**G**SL**MPG	Pancreatic Cancer (93)
	IKAP**NP**PS**VS**TLPPR	Prostate Cancer (94)
GSLEEVSTL ADTAEVSTL ASMEEVSTL	YPHY**SL**PGS**STL**	Lung Cancer (95)
	IKAPNPPS**VSTL**PPR	Prostate Cancer (94)
	CTC**VSTL**SC	Breast Cancer (96)

[a] Selected promiscuous phage clones shown in Appendix 1.

Table 2: Promiscuous Binding Motifs Identified in Other Biopanning Experiments. Identified cross-selected motifs were screened for similar structural motifs between other cancer cell surface markers using the MimoDB v4.3 database. Common motifs are shown in bold. Phage clones that were studied further in this project are shown, where remaining phage clones are shown in Appendix 1.

Preparation	Size Distribution (d.nm)	Zeta Potential (mV)	Doxorubicin Yield	
			µg	%
GSLEEVSTL Modified Lipodox	89.2 ± 0.4	-19.5 ± 1.2	460	84.6
GEFDELMTM Modified Lipodox	90.0 ± 1.1	-17.9 ± 0.2	340	63.4
Unmodified Lipodox	82.5 ± 0.3	-19.1 ± 0.5	540	100

Table 3: Physicochemical Characterization of Phage Protein-Modified Lipodox. Size distribution, zeta potential and doxorubicin yield were measured following phage protein modification.

References

1. Siegel RL, Miller KD, Jemal A. Cancer statistics, 2015. CA: a cancer journal for clinicians 2015;65(1):5-29.
2. Pathology and Genetics of Tumours of the Digestive System. Lyon: World Health Organization; 2000. 219-32 p.
3. Wolfgang CL, Herman JM, Laheru DA, Klein AP, Erdek MA, Fishman EK, et al. Recent progress in pancreatic cancer. Ca-a Cancer Journal for Clinicians 2013;63(5):318-48.
4. Tian H, Callahan CA, DuPree KJ, Darbonne WC, Ahn CP, Scales SJ, et al. Hedgehog signaling is restricted to the stromal compartment during pancreatic carcinogenesis. Proceedings of the National Academy of Sciences of the United States of America 2009;106(11):4254-59.
5. Feig C, Gopinathan A, Neesse A, Chan DS, Cook N, Tuveson DA. The pancreas cancer microenvironment. Clinical cancer research : an official journal of the American Association for Cancer Research 2012;18(16):4266-76.
6. Ettinger DS, Akerley W, Bepler G, Blum MG, Chang A, Cheney RT, et al. Non–Small Cell Lung Cancer. Journal of the National Comprehensive Cancer Network 2010;8(7):740-801.
7. Lengauer C, Kinzler KW, Vogelstein B. Genetic instabilities in human cancers. Nature 1998;396(6712):643-49.
8. Almoguera C, Shibata D, Forrester K, Martin J, Arnheim N, Perucho M. MOST HUMAN CARCINOMAS OF THE EXOCRINE PANCREAS CONTAIN MUTANT C-K-RAS GENES. Cell 1988;53(4):549-54.

9. Mitelman F. CATALOG OF CHROMOSOME-ABERRATIONS IN CANCER. Cytogenetics and Cell Genetics 1983;36(1-2):1-&.

10. Albertson DG, Collins C, McCormick F, Gray JW. Chromosome aberrations in solid tumors. Nature Genetics 2003;34(4):369-76.

11. Axelson H, Fredlund E, Ovenberger M, Landberg G, Pahlman S. Hypoxia-induced dedifferentiation of tumor cells--a mechanism behind heterogeneity and aggressiveness of solid tumors. Seminars in cell & developmental biology 2005;16(4-5):554-63.

12. Sekido Y, Fong KM, Minna JD. Molecular genetics of lung cancer. Annual Review of Medicine-Selected Topics in the Clinical Sciences 2003;54:73-87.

13. Zilfou JT, Lowe SW. Tumor Suppressive Functions of p53. Cold Spring Harbor Perspectives in Biology 2009;1(5):12.

14. Roth JA, Nguyen D, Lawrence DD, Kemp BL, Carrasco CH, Ferson DZ, et al. Retrovirus-mediated wild-type p53 gene transfer to tumors of patients with lung cancer. Nature medicine 1996;2(9):985-91.

15. Shapiro GI, Park JE, Edwards CD, Mao L, Merlo A, Sidransky D, et al. MULTIPLE MECHANISMS OF P16(INK4A) INACTIVATION IN NON-SMALL-CELL LUNG-CANCER CELL-LINES. Cancer research 1995;55(24):6200-09.

16. Riely GJ, Marks J, Pao W. *KRAS* Mutations in Non-Small Cell Lung Cancer. 2009. p 201-05.

17. Karachaliou N, Mayo C, Costa C, Magri I, Gimenez-Capitan A, Molina-Vila MA, et al. KRAS Mutations in Lung Cancer. Clinical Lung Cancer 2013;14(3):205-14.

18. Bardeesy N, DePinho RA. Pancreatic cancer biology and genetics. Nature Reviews Cancer 2002;2(12):897-909.

19. Klimstra DS, Longnecker DS. K-RAS MUTATIONS IN PANCREATIC DUCTAL PROLIFERATIVE LESIONS. American Journal of Pathology 1994;145(6):1547-48.

20. Shields JM, Pruitt K, McFall A, Shaub A, Der CJ. Understanding Ras: 'it ain't over 'til it's over'. Trends in Cell Biology 2000;10(4):147-54.

21. Watanabe M, Nobuta A, Tanaka J, Asaka M. An effect of K-ras gene mutation on epidermal growth factor receptor signal transduction in PANC-1 pancreatic carcinoma cells. International Journal of Cancer 1996;67(2):264-68.

22. McWilliams RR, Wieben ED, Rabe KG, Pedersen KS, Wu YH, Sicotte H, et al. Prevalence of CDKN2A mutations in pancreatic cancer patients: implications for genetic counseling. European Journal of Human Genetics 2011;19(4):472-78.

23. Wang QQ, Ni QC, Wang XD, Zhu HJ, Wang ZW, Huang JF. High expression of RAB27A and TP53 in pancreatic cancer predicts poor survival. Medical Oncology 2015;32(1):9.

24. Heppner GH. TUMOR HETEROGENEITY. Cancer research 1984;44(6):2259-65.

25. Ichim CV, Wells RA. First among equals: The cancer cell hierarchy. Leukemia & Lymphoma 2006;47(10):2017-27.

26. Michor F, Polyak K. The origins and implications of intratumor heterogeneity. Cancer prevention research 2010;3(11):1361-4.

27. Donnenberg VS, Donnenberg AD. Multiple drug resistance in cancer revisited: the cancer stem cell hypothesis. Journal of clinical pharmacology 2005;45(8):872-7.

28. Greaves M, Maley CC. Clonal evolution in cancer. Nature 2012;481(7381):306-13.

29. Junttila MR, de Sauvage FJ. Influence of tumour micro-environment heterogeneity on therapeutic response. Nature 2013;501(7467):346-54.

30. Park CC, Bissell MJ, Barcellos-Hoff MH. The influence of the microenvironment on the malignant phenotype. Molecular Medicine Today 2000;6(8):324-29.

31. Marusyk A, Polyak K. Tumor heterogeneity: causes and consequences. Biochimica et biophysica acta 2010;1805(1):105-17.

32. Evans DB, Abbruzzese JL, Willett CG. Cancer: Principles & Practice of Oncology. DeVita VT, Hellman SA, Rosenberg, editors. Philadelphia: Lippincott and Wilkins; 2001.

33. Pliarchopoulou K, Pectasides D. Pancreatic cancer: Current and future treatment strategies. Cancer Treatment Reviews 2009;35(5):431-36.

34. Schiller JH. Current standards of care in small-cell and non-small-cell lung cancer. Oncology 2001;61:3-13.

35. Sahoo SK, Labhasetwar V. Nanotech approaches to delivery and imaging drug. Drug Discovery Today 2003;8(24):1112-20.

36. Kawasaki ES, Player A. Nanotechnology, nanomedicine, and the development of new, effective therapies for cancer. Nanomedicine: Nanotechnology, Biology, and Medicine 2005;1(2):101-09.

37. Nakamura H, Jun F, Maeda H. Development of next-generation macromolecular drugs based on the EPR effect: challenges and pitfalls. Expert opinion on drug delivery 2015;12(1):53-64.

38. Yin H, Liao L, Fang J. Enhanced Permeability and Retention (EPR) Effect Based Tumor Targeting: The Concept, Application and Prospect. JSM Clinical Oncology and Research 2014;2(1):1010.

39. Prokop A, Davidson JM. Nanovehicular intracellular delivery systems. J Pharm Sci 2008;97(9):3518-90.

40. Prabhakar U, Maeda H, Jain RK, Sevick-Muraca EM, Zamboni W, Farokhzad OC, et al. Challenges and Key Considerations of the Enhanced Permeability and Retention Effect for Nanomedicine Drug Delivery in Oncology. Cancer research 2013;73(8):2412-17.

41. Haley B, Frenkel E. Nanoparticles for drug delivery in cancer treatment. Urologic oncology 2008;26(1):57-64.

42. Veiseh O, Gunn JW, Zhang M. Design and fabrication of magnetic nanoparticles for targeted drug delivery and imaging. Advanced drug delivery reviews 2010;62(3):284-304.

43. Napoli C, Balestrieri A, Ignarro LJ. Therapeutic approaches in vascular repair induced by adult bone marrow cells and circulating progenitor endothelial cells. Current pharmaceutical design 2007;13(31):3245-51.

44. Sun J, Kim DH, Guo Y, Teng ZG, Li YJ, Zheng LF, et al. A c(RGDfE) conjugated multi-functional nanomedicine delivery system for targeted pancreatic cancer therapy. J Mater Chem B 2015;3(6):1049-58.

45. Smith LE, Denissenko MF, Bennett WP, Li H, Amin S, Tang M, et al. Targeting of lung cancer mutational hotspots by polycyclic aromatic hydrocarbons. Journal of the National Cancer Institute 2000;92(10):803-11.

46. Zhao G, Rodriguez BL. Molecular targeting of liposomal nanoparticles to tumor microenvironment. International journal of nanomedicine 2013;8:61-71.

47. Danhier F, Feron O, Preat V. To exploit the tumor microenvironment: Passive and active tumor targeting of nanocarriers for anti-cancer drug delivery. Journal of Controlled Release 2010;148(2):135-46.

48. Kim DK, Dobson J. Nanomedicine for targeted drug delivery. J Mater Chem 2009;19(35):6294-307.

49. Torchilin V. Tumor delivery of macromolecular drugs based on the EPR effect. Advanced drug delivery reviews 2011;63(3):131-5.

50. Prabhakar U, Maeda H, Jain RK, Sevick-Muraca EM, Zamboni W, Farokhzad OC, et al. Challenges and key considerations of the enhanced permeability and retention effect for nanomedicine drug delivery in oncology. Cancer research 2013;73(8):2412-7.

51. Kumar Khanna V. Targeted delivery of nanomedicines. ISRN Pharmacol 2012;2012:571394.

52. Bae YH. Drug targeting and tumor heterogeneity. Journal of Controlled Release 2009;133(1):2-3.

53. Newton JR, Kelly KA, Mahmood U, Weissleder R, Deutscher SL. In vivo selection of phage for the optical Imaging of PC-3 human prostate carcinoma in mice. Neoplasia 2006;8(9):772-80.

54. Bedi D, Gillespie JW, Petrenko VA. Selection of pancreatic cancer cell-binding landscape phages and their use in development of anticancer nanomedicines. Protein engineering, design & selection : PEDS 2014;27(7):235-43.

55. Fagbohun OA, Bedi D, Grabchenko NI, Deinnocentes PA, Bird RC, Petrenko VA. Landscape phages and their fusion proteins targeted to breast cancer cells. Protein Eng Des Sel 2012;25(6):271-83.

56. Smith GP, Petrenko VA. Phage display. Chem Rev 1997;97(2):391-410.

57. Rakonjac J, Bennett NJ, Spagnuolo J, Gagic D, Russel M. Filamentous bacteriophage: biology, phage display and nanotechnology applications. Current issues in molecular biology 2011;13(2):51-76.

58. Deng LW, Perham RN. Delineating the site of interaction on the pIII protein of filamentous bacteriophage fd with the F-pilus of Escherichia coli. Journal of molecular biology 2002;319(3):603-14.

59. Bennett NJ, Rakonjac J. Unlocking of the filamentous bacteriophage virion during infection is mediated by the C domain of pIII. Journal of molecular biology 2006;356(2):266-73.

60. Clarke M, Maddera L, Harris RL, Silverman PM. F-pili dynamics by live-cell imaging. Proceedings of the National Academy of Sciences of the United States of America 2008;105(46):17978-81.

61. Russel M, Model P. Genetic analysis of the filamentous bacteriophage packaging signal and of the proteins that interact with it. Journal of virology 1989;63(8):3284-95.

62. Feng JN, Russel M, Model P. A permeabilized cell system that assembles filamentous bacteriophage. Proceedings of the National Academy of Sciences of the United States of America 1997;94(8):4068-73.

63. Rakonjac J, Feng J, Model P. Filamentous phage are released from the bacterial membrane by a two-step mechanism involving a short C-terminal fragment of pIII. Journal of molecular biology 1999;289(5):1253-65.

64. Tikunova NV, Morozova VV. Phage display on the base of filamentous bacteriophages: application for recombinant antibodies selection. Acta naturae 2009;1(3):20-8.

65. Kuzmicheva GA, Jayanna PK, Sorokulova IB, Petrenko VA. Diversity and censoring of landscape phage libraries. Protein engineering, design & selection : PEDS 2009;22(1):9-18.

66. Petrenko VA, Smith GP, Gong X, Quinn T. A library of organic landscapes on filamentous phage. Protein Engineering 1996;9(9):797-801.

67. Kuzmicheva GA, Jayanna PK, Eroshkin AM, Grishina MA, Pereyaslavskaya ES, Potemkin VA, et al. Mutations in fd phage major coat protein modulate affinity of the displayed peptide. Protein engineering, design & selection : PEDS 2009;22(10):631-9.

68. Brigati JR, Petrenko VA. Thermostability of landscape phage probes. Analytical and bioanalytical chemistry 2005;382(6):1346-50.

69. Gandra N, Wang DD, Zhu Y, Mao C. Virus-mimetic cytoplasm-cleavable magnetic/silica nanoclusters for enhanced gene delivery to mesenchymal stem cells. Angewandte Chemie 2013;52(43):11278-81.

70. Deutscher SL. Phage display in molecular imaging and diagnosis of cancer. Chem Rev 2010;110(5):3196-211.

71. Rajotte D, Arap W, Hagedorn M, Koivunen E, Pasqualini R, Ruoslahti E. Molecular heterogeneity of the vascular endothelium revealed by in vivo phage display. The Journal of clinical investigation 1998;102(2):430-7.

72. Ruoslahti E. Targeting tumor vasculature with homing peptides from phage display. Seminars in cancer biology 2000;10(6):435-42.

73. Bedi D, Gillespie JW, Petrenko VA, Jr., Ebner A, Leitner M, Hinterdorfer P, et al. Targeted delivery of siRNA into breast cancer cells via phage fusion proteins. Mol Pharm 2013;10(2):551-9.

74. Lang Q, Wang F, Yin L, Liu M, Petrenko VA, Liu A. Specific probe selection from landscape phage display library and its application in enzyme-linked immunosorbent assay of free prostate-specific antigen. Analytical chemistry 2014;86(5):2767-74.

75. Jayanna PK, Bedi D, Deinnocentes P, Bird RC, Petrenko VA. Landscape phage ligands for PC3 prostate carcinoma cells. Protein Eng Des Sel 2010;23(6):423-30.

76. Wang F, Liu P, Sun L, Li C, Petrenko VA, Liu A. Bio-mimetic nanostructure self-assembled from Au@Ag heterogeneous nanorods and phage fusion proteins for targeted tumor optical detection and photothermal therapy. Scientific reports 2014;4:6808.

77. Jayanna PK, Bedi D, Gillespie JW, DeInnocentes P, Wang T, Torchilin VP, et al. Landscape phage fusion protein-mediated targeting of nanomedicines enhances

their prostate tumor cell association and cytotoxic efficiency. Nanomedicine-Nanotechnology Biology and Medicine 2010;6(4):538-46.

78. Wang T, D'Souza GG, Bedi D, Fagbohun O, Potturi LP, Papahadjopoulos-Sternberg B, et al. Enhanced binding and killing of target tumor cells by drug-loaded liposomes modified with tumor-specific phage fusion coat protein. Nanomedicine (Lond) 2010;5(4):563-74.

79. Wang T, Yang S, Mei LA, Parmar CK, Gillespie JW, Praveen KP, et al. Paclitaxel-loaded PEG-PE-based micellar nanopreparations targeted with tumor-specific landscape phage fusion protein enhance apoptosis and efficiently reduce tumors. Molecular cancer therapeutics 2014;13(12):2864-75.

80. Samoylova TI, Petrenko VA, Morrison NE, Globa LP, Baker HJ, Cox NR. Phage probes for malignant glial cells. Molecular cancer therapeutics 2003;2(11):1129-37.

81. Guo YE, Ma CX, Li CY, Wu JL, Zhang D, Han JJ, et al. Screening and identification of a specific peptide binding to hepatocellular carcinoma cells from a phage display peptide library. Journal of Peptide Science 2014;20(3):196-202.

82. Smith GP, Petrenko VA, Matthews LJ. Cross-linked filamentous phage as an affinity matrix. Journal of Immunological Methods 1998;215(1-2):151-61.

83. Brigati JR, Samoylova TI, Jayanna PK, Petrenko VA. Phage display for generating peptide reagents. Current protocols in protein science / editorial board, John E Coligan [et al] 2008;Chapter 18:Unit 18.9.

84. Mandava S, Makowski L, Devarapalli S, Uzubell J, Rodi DJ. RELIC--a bioinformatics server for combinatorial peptide analysis and identification of protein-ligand interaction sites. Proteomics 2004;4(5):1439-60.

85. Jayanna PK, Torchilin VP, Petrenko VA. Liposomes targeted by fusion phage proteins. Nanomedicine-Nanotechnology Biology and Medicine 2009;5(1):83-89.

86. Gillespie JW, Gross AL, Puzyrev AT, Bedi D, Petrenko VA. Combinatorial synthesis and screening of cancer cell-specific nanomedicines targeted via phage fusion proteins. Frontiers in Microbiology 2015;6.

87. Khare V, Alam N, Saneja A, Dubey RD, Gupta PN. Targeted Drug Delivery Systems for Pancreatic Cancer. J Biomed Nanotechnol 2014;10(12):3462-82.

88. Chandolu V, Dass CR. Treatment of lung cancer using nanoparticle drug delivery systems. Current drug discovery technologies 2013;10(2):170-6.

89. Koivunen E, Gay DA, Ruoslahti E. SELECTION OF PEPTIDES BINDING TO THE ALPHA-5-BETA-1 INTEGRIN FROM PHAGE DISPLAY LIBRARY. Journal of Biological Chemistry 1993;268(27):20205-10.

90. Wang T, Petrenko VA, Torchilin VP. Paclitaxel-Loaded Polymeric Micelles Modified with MCF-7 Cell-Specific Phage Protein: Enhanced Binding to Target Cancer Cells and Increased Cytotoxicity. Molecular Pharmaceutics 2010;7(4):1007-14.

91. Petrenko VA, Jayanna PK. Phage protein-targeted cancer nanomedicines. FEBS letters 2014;588(2):341-9.

92. te Velde EA, Veerman T, Subramaniam V, Ruers T. The use of fluorescent dyes and probes in surgical oncology. Ejso 2010;36(1):6-15.

93. Huang CH, Liu XY, Rehemtulla A, Lawrence TS. Identification of peptides that bind to irradiated pancreatic tumor cells. International Journal of Radiation Oncology Biology Physics 2005;62(5):1497-503.

94. Newton-Northup JR, Figueroa SD, Deutscher SL. Streamlined In Vivo Selection and Screening of Human Prostate Carcinoma Avid Phage Particles for Development of Peptide Based In Vivo Tumor Imaging Agents. Combinatorial Chemistry & High Throughput Screening 2011;14(1):9-21.

95. Zang LQ, Shi L, Guo J, Pan Q, Wu W, Pan XD, et al. Screening and Identification of a peptide specifically targeted to NCI-H1299 from a phage display peptide library. Cancer Letters 2009;281(1):64-70.

96. Arap W, Pasqualini R, Ruoslahti E. Cancer treatment by targeted drug delivery to tumor vasculature in a mouse model. Science 1998;279(5349):377-80.

97. Lee S-M, Lee E-J, Hong H-Y, Kwon M-K, Kwon T-H, Choi J-Y, et al. Targeting bladder tumor cells in vivo and in the urine with a peptide identified by phage display. Molecular Cancer Research 2007;5(1):11-19.

98. Krag DN, Shukla GS, Shen GP, Pero S, Ashikaga T, Fuller S, et al. Selection of tumor-binding ligands in cancer patients with phage display libraries. Cancer research 2006;66(15):7724-33.

99. Dane KY, Chan LA, Rice JJ, Daugherty PS. Isolation of cell specific peptide ligands using fluorescent bacterial display libraries. Journal of Immunological Methods 2006;309(1-2):120-29.

100. Thomas WD, Golomb M, Smith GP. Corruption of phage display libraries by target-unrelated clones: Diagnosis and countermeasures. Analytical Biochemistry 2010;407(2):237-40.

101. Lu RM, Chen MS, Chang DK, Chiu CY, Lin WC, Yan SL, et al. Targeted Drug Delivery Systems Mediated by a Novel Peptide in Breast Cancer Therapy and Imaging. PloS one 2013;8(6):13.

102. Wang J, Dong B, Chen BT, Jiang ZL, Song HW. Selective photothermal therapy for breast cancer with targeting peptide modified gold nanorods. Dalton transactions 2012;41(36):11134-44.

103. Kelly KA, Jones DA. Isolation of a colon tumor specific binding peptide using phage display selection. Neoplasia 2003;5(5):437-44.

104. Morita Y, Mamiya K, Yamamura S, Tamiya E. Selection and properties for the recognition of P19 embryonic carcinoma stem cells. Biotechnology Progress 2006;22(4):974-78.

105. Derda R, Musah S, Orner BP, Klim JR, Li LY, Kiessling LL. High-Throughput Discovery of Synthetic Surfaces That Support Proliferation of Pluripotent Cells. Journal of the American Chemical Society 2010;132(4):1289-95.

106. Nguyen HD, Phan TTP, Carraz M, Brunsveld L. Estrogen Receptor alpha/beta-cofactor motif interactions; interplay of tyrosine 537/488 phosphorylation and LXXLL motifs. Molecular Biosystems 2012;8(12):3134-41.

107. Chang CY, Norris JD, Gron H, Paige LA, Hamilton PT, Kenan DJ, et al. Dissection of the LXXLL nuclear receptor-coactivator interaction motif using

combinatorial peptide libraries: Discovery of peptide antagonists of estrogen receptors alpha and beta. Molecular and cellular biology 1999;19(12):8226-39.

108. Kang JQ, Zhao GH, Lin T, Tang SH, Xu GH, Hu SJ, et al. A peptide derived from phage display library exhibits anti-tumor activity by targeting GRP78 in gastric cancer multidrug resistance cells. Cancer Letters 2013;339(2):247-59.

109. Han Z, Fu A, Wang H, Diaz R, Geng L, Onishko H, et al. Noninvasive assessment of cancer response to therapy. Nature medicine 2008;14(3):343-49.

110. Healy JM, Murayama O, Maeda T, Yoshino K, Sekiguchi K, Kikuchi M. PEPTIDE LIGANDS FOR INTEGRIN ALPHA(V)BETA(3) SELECTED FROM RANDOM PHAGE DISPLAY LIBRARIES. Biochemistry 1995;34(12):3948-55.

111. Kraft S, Diefenbach B, Mehta R, Jonczyk A, Luckenbach GA, Goodman SL. Definition of an unexpected ligand recognition motif for alpha nu beta 6 integrin. Journal of Biological Chemistry 1999;274(4):1979-85.

112. Murayama O, Nishida H, Sekiguchi K. Novel peptide ligands for integrin alpha 6 beta 1 selected from a phage display library. Journal of Biochemistry 1996;120(2):445-51.

113. Koivunen E, Ranta TM, Annila A, Taube S, Uppala A, Jokinen M, et al. Inhibition of beta(2) integrin-mediated leukocyte cell adhesion by leucine-leucine-glycine motif-containing peptides. Journal of Cell Biology 2001;153(5):905-15.

114. Li RH, Hoess RH, Bennett JS, DeGrado WF. Use of phage display to probe the evolution of binding specificity and affinity in integrins. Protein Engineering 2003;16(1):65-72.

115. Matsumura N, Tsuji T, Sumida T, Kokubo M, Onimaru M, Doi N, et al. mRNA display selection of a high-affinity, Bcl-X-L-specific binding peptide. Faseb Journal 2010;24(7):2201-10.

116. Takahashi S, Mok H, Parrott MB, Marini FC, Andreeff M, Brenner MK, et al. Selection of chronic lymphocytic leukemia binding peptides. Cancer research 2003;63(17):5213-17.

117. McGuire MJ, Samli KN, Chang YC, Brown KC. Novel ligands for cancer diagnosis: Selection of peptide ligands for identification and isolation of B-cell lymphomas. Experimental Hematology 2006;34(4):443-52.

118. Tu XG, Zang LQ, Lan DY, Liang WC. Screening and identification of a peptide specifically targeted to NCI-H1299 cells from a phage display peptide library. Molecular Medicine Reports 2009;2(6):1005-10.

119. Lee TY, Wu HC, Tseng YL, Lin CT. A novel peptide specifically binding to nasopharyngeal carcinoma for targeted drug delivery. Cancer research 2004;64(21):8002-08.

120. Slobbe R, Poels L, Tendam G, Boerman O, Nieland L, Leunissen J, et al. ANALYSIS OF IDIOTOPE STRUCTURE OF OVARIAN-CANCER ANTIBODIES - RECOGNITION OF THE SAME EPITOPE BY 2 MONOCLONAL-ANTIBODIES DIFFERING MAINLY IN THEIR HEAVY-CHAIN VARIABLE SEQUENCES. Clinical and experimental immunology 1994;98(1):95-103.

121. Ma CY, Yin GF, Yan DH, He XL, Zhang L, Wei Y, et al. A novel peptide specifically targeting ovarian cancer identified by in vivo phage display. Journal of Peptide Science 2013;19(12):730-36.

122. Romanov VI, Durand DB, Petrenko VA. Phage display selection of peptides that affect prostate carcinoma cells attachment and invasion. Prostate 2001;47(4):239-51.

123. Kamada H, Okamota T, Kawamura M, Shibata H, Abe Y, Ohkawa A, et al. Creation of novel cell-penetrating peptides for intracellular drug delivery using systematic phage display technology originated from tat transduction domain. Biological & Pharmaceutical Bulletin 2007;30(2):218-23.

124. Bockmann M, Hilken G, Schmidt A, Cranston AN, Tannapfel A, Drosten M, et al. Novel SRESPHP peptide mediates specific binding to primary medullary thyroid carcinoma after systemic injection. Human Gene Therapy 2005;16(11):1267-75.

Appendix 1

Promiscuous Binding Motifs Identified in Other Biopanning Experiments.

Promiscuous Peptide	Motif-containing peptides from other selected peptides	Target/Reference
V**DGR**LGDEH	CVNN**DGR**LC	Bladder Cancer (97)
GNM**AE**ITS**L**	NNRACFRTSK**GN**P**AE**CPY**L**G	Breast Cancer (98)
D**GR**S**IV**GDE	WARVLLIE**GR**L**IV**CE	Breast Cancer (99)
D**GR**DH**SG**QD	CN**GR**CV**SG**CAGRC	Breast Cancer (96)
D**GRSV**MESD	AVAG**GRSV**VDARVAR	Breast Cancer (100)
D**GR**FG**VD**GS	AVAG**GR**SV**VD**ARVAR	Breast Cancer (100)
GSLAETSTL	**GSLA**CQNIVVCVKKQCNALC	Breast Cancer (98)
DGRDG**GTGS**	**GTGS**CGYGKLHTGYWCSYFP	Breast Cancer (98)
V**IY**P**GV**GED	QN**IY**A**GV**PMISF	Breast Cancer (101)
V**LR**G**DD**MNN	VN**LR**M**DD**HDWSR	Breast Cancer (102)
DGR**MGSE**VS	LPNFCMDTSGRAGPLC**MGSE**	Breast Cancer (98)
EYDKE**TSTL**	INLQ**TSTL**MSHT	Breast Cancer (102)
GSLAE**TSTL**	INLQ**TSTL**MSHT	Breast Cancer (102)
ADTAE**VSTL**	CTC**VSTL**SC	Breast Cancer (96)
ASMEE**VSTL**	CTC**VSTL**SC	Breast Cancer (96)
VD**WD**N**VS**ES	W**WD**M**VS**DRYIWKPVK	Breast Cancer (99)
EDA**RTAA**MA	CSL**RTAA**AC	Colon Cancer (103)
DPLAE**VTTL**	C**VTTL**NLTC	Colon Cancer (103)
V**GI**D**EQ**RAD	M**GI**A**EQ**LMH	Embryonic Cancer Cells (104)
AFD**PD**LH**LN**	FAKS**PD**VS**LN**PS	Embryonic Cancer Cells (105)
R**VP**G**SY**SID	TTRQ**VP**V**SY**TSS	Embryonic Cancer Cells (104)
AVGSEEALL	RG**AVGS**SLVCLLTYSDNVC	Estrogen receptor (106)
AT**GEPG**MDA	PV**GEPG**LLWRLLSAPVWRE	Estrogen receptor (107)
AV**GS**EE**AL**L	DD**GS**HI**AL**HPLLFGHLVPF	Estrogen receptor (106)
AV**GS**EEA**LL**	SSFCF**GS**LYS**LL**ATHRCSS	Estrogen receptor (106)
AV**GS**EEA**LL**	CSDG**GS**ILT**LL**LCSNVSRA	Estrogen receptor (106)
AV**GS**EEA**LL**	IIDDH**GS**LLS**LL**PLIGTSF	Estrogen receptor (106)
AV**GS**EEA**LL**	CSDG**GS**ILLL**LL**CSNVSRA	Estrogen receptor (106)
AV**GS**EEA**LL**	DHHTN**GS**LYF**LL**SNNGDNN	Estrogen receptor (106)
AFD**PD**L**H**LN	Y**PD**T**H**LLLYSLLLPDSANA	Estrogen receptor (106)
A**VG**SEEA**LL**	ALNSN**VG**LVRL**LL**RDDFSS	Estrogen receptor (106)
AFDP**DL**H**LN**	APKYSLS**DL**Y**LN**	Gastric Cancer (108)

DP**LA**EV**TT**L	NSSQ**LA**PY**TT**HR	Gastric Cancer (108)
V**SY**L**ES**EES	FTF**SY**A**ES**VSYF	Gastric Cancer (108)
AD**TA**EV**ST**L	E**TA**PL**ST**MLSPY	Gastric Cancer (108)
V**TFDP**YDNN	Y**TFDP**QIRPAGL	Gastric Cancer (108)
D**GR**DG**G**T**GS**	S**GR**KV**G**S**GS**SV	Glioblastoma (109)
V**LRGD**DMNN	S**LRGD**GSSV	Glioblastoma (109)
V**LRGD**DMNN	E**LRGD**SLP	Glioma (80)
AFP**GD**ESDT	**AF**R**GD**S	Integrin (110)
AFDP**DLHL**N	RG**DLHL**	Integrin (89)
AFP**GD**ES**DT**	R**GD**SF**DT**RYAPL	Integrin (111)
AT**G**E**PG**M**DA**	VGFLGLKR**G**P**PG**V**DA**	Integrin (112)
AV**GSEE**ALL	CWKLL**GSEE**EC	Integrin (113)
V**LRGD**DMNN	S**LRGD**HRVRWVLTPH	Integrin (110)
V**LRGD**DMNN	QY**LRGD**	Integrin (110)
V**LRGD**DMNN	NG**LRGD**	Integrin (110)
V**LRGD**DMNN	RA**LRGD**RGWIVFWDP	Integrin (110)
V**LRGD**DMNN	SR**LRGD**	Integrin (110)
VL**RGDD**MNN	HLA**RGDD**LTY	Integrin (114)
A**TY**N**ES**VNE	VSRGD**TY**V**ES**	Integrin (114)
VLRGDDMNN	**VLRGD**N	Integrin (110)
EDART**AAMA**	MWVHS**AAMA**TGLASRM	Leukemia (115)
AVGSE**EALL**	GWWQFWDWSARRQDRG**EALL**	Leukemia (116)
GS**FS**EA**SV**S	ARA**FS**YW**SV**TDTERVKFFVP	Leukemia (116)
GSLA**ET**STL	EFGH**GS**PY**ET**RQHSQARRWL	Leukemia (116)
DGRDG**GTGS**	WLSEAGPVVTVRALR**GTGS**W	Leukemia (117)
GYP**IG**GDTT	MAQKWGGGQALQ**GY**H**IG**ANA	Leukemia (116)
VIY**PG**V**GE**D	MARTVTANV**PG**M**GE**GMVVVP	Leukemia (116)
DG**RHL**DQ**VD**	**RHL**LL**VD**RLRAIALLL	Leukemia (115)
A**TG**EPGM**DA**	RTS**TG**PEAR**DA**WMWYWKPPA	Leukemia (116)
VGW**SP**EVPD	GGHGRVLWPDGWFSL**VG**I**SP**	Leukemia (116)
GEEGE**YIAA**	SQRSTM**YIAA**VLRWLA	Leukemia (115)
VEEGG**YIAA**	SQRSTM**YIAA**VLRWLA	Leukemia (115)
DGR**SV**MESD	SLRG**DG**S**SV**	Lung Cancer (109)
D**GR**DG**G**T**GS**	S**GR**KV**G**S**GS**SV	Lung Cancer (109)
DN**GR**E**VG**ND	S**GR**K**VG**SGSSV	Lung Cancer (109)
ED**IS**E**L**N**TL**	AHRHP**IS**F**L**S**TL**	Lung Cancer (95) (118)
V**LRGD**DMNN	S**LRGD**GSSV	Lung Cancer (109)
DG**R**M**GSEV**S	SVV**R**D**GSEV**	Lung Cancer (109)
G**SL**EEV**STL**	YPHY**SL**PGS**STL**	Lung Cancer (95)
E**VS**VEE**INL**	S**VS**LPY**INL**ATH	Nasopharyngeal Cancer (119)
VGD**AGHS**ME	AL**AGHS**	Ovarian Cancer (120)

DG**RYIG**DND	S**RYIG**S	Ovarian Cancer (120)
EDI**SELN**TL	YP**SELN**VRTPHR	Ovarian Cancer (121)
VD**WS**TD**GV**D	**WS**GP**GV**WGASVK	Ovarian Cancer (121)
DYNP**EL**V**SL**	NHTT**EL**G**SL**MPG	Pancreatic Cancer (93)
ADG**RD**H**YSD**	V**AD**D**RD-YSD**	Prostate Cancer (75)
AEYGESV**NA**	**AEYGES**G**NA**	Prostate Cancer (75)
AEYGESVNA	**AEYGESV**LI	Prostate Cancer (75)
AEYGESVNA	**AEYGESVNA**	Prostate Cancer (75)
AEYGESV**NA**	**AEYG**ERG**NA**	Prostate Cancer (75)
DGR**AYDVN**E	G**AYDVN**VND	Prostate Cancer (75)
AT**Y**N**ESVN**E	**A**E**Y**G**ESVN**A	Prostate Cancer (75)
DPL**A**EV**TTL**	**DP**R**A**TT**TTL**	Prostate Cancer (122)
DPRVES**MS**G	**DPR**IAT**MS**	Prostate Cancer (122)
E**D**A**RTAAMA**	**D**P**RTAAMA**	Prostate Cancer (122)
AFGED**DYSD**	VADDR**DYSD**	Prostate Cancer (75)
GDYT**EA**V**GA**	**EA**A**GA**NIAP	Prostate Cancer (75)
EPWSP**TM**GD	TNTNCGTDL**EP**CVS**TM**	Prostate Cancer (94)
GPYVGDL**DS**	**GP**NWAEG**DS**	Prostate Cancer (75)
DELI**LVGT**G	SVGGWFRQH**LVGT**RM	Prostate Cancer (53)
DY**NP**EL**VS**L	IKAP**NP**PS**VS**TLPPR	Prostate Cancer (94)
ATGE**PG**M**DA**	T**PG**L**DA**AFWSLGSE	Prostate Cancer (94)
DG**RA**D**LS**YD	E**RA**P**LS**VE	Prostate Cancer (75)
DG**RD**GGT**GS**	VMVPYSV**RD**SLF**GS**F	Prostate Cancer (53)
ADTAE**VSTL**	IKAPNPPS**VSTL**PPR	Prostate Cancer (94)
ASMEE**VSTL**	IKAPNPPS**VSTL**PPR	Prostate Cancer (94)
GSLEE**VSTL**	IKAPNPPS**VSTL**PPR	Prostate Cancer (94)
DHV**WAEGDS**	GPN**WAEGDS**	Prostate Cancer (75)
AD**GR**D**HY**SD	**GR**N**HY**IQRDNPVS	Skin Cancer (123)
DHY**GSSS**ES	**GSSS**WWQRWWPPW	Skin Cancer (123)
GSA**SV**DM**DM**	GLRKVPQ**SV**PP**DM**	Skin Cancer (123)
AFDP**DL**H**LN**	CS**DL**Y**LN**FC	Thyroid Cancer (124)

Appendix Table 1: **Promiscuous Binding Motifs Identified in Other Biopanning Experiments.** Selected motifs were screened for similar structural motifs between other known cell surface markers using the MimoDB v4.3 database. Common motifs are shown in bold.